

## Constraining the Properties of GRB Accreting Magnetar with $R/I$ Evolutionary Effects Using *Swift*/XRT Data

LIN LAN,<sup>1</sup> HE GAO,<sup>2,3</sup> LITAO ZHAO,<sup>4</sup> SHUNKE AI,<sup>5</sup> JIE LIN,<sup>6</sup> LONG LI,<sup>7</sup> LANG XIE,<sup>7</sup> LI-PING XIN,<sup>1</sup> AND JIAN-YAN WEI<sup>1</sup>

<sup>1</sup>*CAS Key Laboratory of Space Astronomy and Technology, National Astronomical Observatories, Chinese Academy of Sciences, Beijing 100012, People's Republic of China; lanlin@bao.ac.cn*

<sup>2</sup>*School of Physics and Astronomy, Beijing Normal University, Beijing 100875, People's Republic of China; gaohe@bnu.edu.cn*

<sup>3</sup>*Institute for Frontier in Astronomy and Astrophysics, Beijing Normal University, Beijing 102206, People's Republic of China*

<sup>4</sup>*School of Mathematics and Science, Hebei GEO University, Shijiazhuang, People's Republic of China*

<sup>5</sup>*Niels Bohr International Academy and DARK, Niels Bohr Institute, University of Copenhagen, Blegdamsvej 17, 2100, Copenhagen, Denmark*

<sup>6</sup>*Department of Astronomy, Xiamen University, Xiamen, Fujian 361005, People's Republic of China*

<sup>7</sup>*Department of Physics, School of Physics and Materials Science, Nanchang University, Nanchang 330031, People's Republic of China*

### ABSTRACT

A newly born millisecond magnetar has been proposed as one possible central engine of some long gamma-ray bursts (LGRBs) with X-ray plateau emission. In this work, we used a universal correlation between the initial spin period ( $P_0$ ) and the surface magnetic field ( $B_p$ ) of the newborn magnetar based on an LGRB sample in Lan et al. (2025) to explore the propeller properties of accreting magnetar with  $R/I$  evolutionary effects. We found that the  $B_p - P_0$  relation is approximately consistent with  $B_p \propto P_{\text{eq}}^{7/6}$ . Here,  $P_{\text{eq}}$  is the equilibrium spin period in magnetic propeller model, where the electromagnetic dipole radiation and the propeller mechanism jointly modulate the spin evolution of newborn magnetar. The  $B_p - P_0$  relation indicates that  $P_0$  constrained by X-ray plateau data may not be the true initial spin period of newborn magnetar, but had reached an equilibrium spin period via fallback accretion in the propeller model. The magnetar accretion rate in our LGRBs is in the range of  $\dot{M} \sim 10^{-5} - 10^{-2} M_{\odot} \text{ s}^{-1}$  by incorporating  $R/I$  evolutionary effects, and using the transition relation between gravitational mass  $M_g$  and baryonic mass  $M_b$  in different equation of states and X-ray radiation efficiencies. Such accretion rates ensure that the accreting magnetars in our sample survive until reaching the equilibrium spin period, and the accretion rate is one order of magnitude lower compared to the statistical results in Stratta et al. (2018) and Lin et al. (2020b), which used the constant  $R/I/M_g$  scenario. The fallback rate of progenitor envelope materials onto the magnetar accretion disk for our LGRBs is compatible with the theoretical mass fallback rate of some low-metallicity progenitors. We suggested that adopting a constant  $R/I/M_g$  scenario for modeling the propeller regime in accreting magnetar results in a higher mass accretion rate, which may impair our understanding of the physical nature and its surroundings of accreting magnetar, and that the low-metallicity progenitors can provide enough material to satisfy the accretion requirements of the newborn accreting magnetar in LGRBs.

**Keywords:** gamma-ray burst: general - magnetars

### 1. INTRODUCTION

Gamma-ray bursts (GRBs), one of the most violent explosions in the universe, with a huge amount of isotropic emission energy  $E_{\gamma, \text{iso}}$  from  $\sim 10^{46}$  erg to  $\sim 10^{55}$  erg (Woosley & Bloom 2006; Kumar & Zhang 2015; Zhang 2018; Lan et al. 2023). In general, it is thought to originate from massive star collapse (for long GRBs; LGRBs) or merger

Corresponding author: Lin Lan  
lanlin@bao.ac.cn

Corresponding author: He Gao  
gaohe@bnu.edu.cn

of binary compact stars (for short GRBs; SGRBs). Within post-collapse or post-merger, two competing types of GRB central engine would be formed and power a relativistic outflow (Paczynski 1986; Eichler et al. 1989; Usov 1992; Woosley 1993; Thompson 1994; Dai & Lu 1998a,b; MacFadyen & Woosley 1999; Zhang & Mészáros 2001; Metzger et al. 2008; Zhang 2011): one is a hyper-accreting stellar-mass black hole (BH) via neutrino-anti-neutrino annihilation (Ruffert et al. 1997; Popham et al. 1999; Chen & Beloborodov 2007; Lei et al. 2009, 2013; Liu et al. 2017) or Blandford-Znajek mechanism (Blandford & Znajek 1977; Lee et al. 2000; Li 2000) to launch a relativistic outflow, and the other is a rapidly spinning, strongly magnetized neutron star (NS, also called millisecond magnetar) via losing its rotational energy to power a relativistic outflow (Usov 1992; Thompson 1994; Dai & Lu 1998a,b; Zhang & Mészáros 2001; Metzger et al. 2008, 2011; Bucciantini et al. 2012; Lü & Zhang 2014; Lü et al. 2015). The observed  $\gamma$ -ray prompt emission and multiband afterglow emission can be explained by internal shocks/dissipated photosphere/magnetic dissipation models and synchrotron emission mechanism from elegant external shocks model, respectively (Thompson 1994; Rees & Meszaros 1994; Mészáros & Rees 1997; Sari et al. 1998; Kobayashi 2000; Mészáros 2002; Zhang & Mészáros 2004; Rees & Mészáros 2005; Pe’er et al. 2006; Zhang & Yan 2011; Gao et al. 2013; Gao & Zhang 2015; Kumar & Zhang 2015; Zhang 2018).

Theoretically, it is widely accepted that newborn millisecond magnetars are formed after the mergers of binary NSs or the core collapses of massive stars, accompanied by GRBs with strong X-ray plateau emission, and strong gravitational wave (GW) radiation may be present during the X-ray plateau phase due to a large ellipticity and a high spin (Dai & Lu 1998a,b; Zhang & Mészáros 2001; Corsi & Mészáros 2009; Metzger et al. 2011; Fan et al. 2013a,b; Metzger & Piro 2014). With the successful launch of Neil Gehrels *Swift* Observatory (Gehrels et al. 2004), the early-time afterglow emissions of GRBs have been revealed, and abundant X-ray observation data have been collected. A good fraction of the X-ray afterglows (LGRBs and SGRBs) pose a long-lasting plateau emission feature, which seems to coincide with the prediction of newborn magnetar central engine (Dai & Lu 1998a,b; Zhang & Mészáros 2001; Metzger et al. 2011; Gompertz et al. 2013, 2014; Rowlinson et al. 2013, 2014; Lü & Zhang 2014; Metzger & Piro 2014; Lü et al. 2015). The electromagnetic (EM) dipole emission of newborn magnetar generates a Poynting flux that can undergo magnetic energy dissipation processes with high efficiency (Zhang & Yan 2011) and inject additional energy into the GRB to induce transient X-ray plateau emission, and the transient X-ray plateau luminosity and temporal evolution are highly dependent on the spin-down behavior of the newborn magnetar.

In previous studies, the magnetar remnants of GRB were usually treated as isolated NSs with a constant spin-down rate and therefore a constant level of EM emission. The physical properties and lifetime of the newly born magnetar could be inferred from the observed multiband afterglow morphological characteristics and plateau data (Troja et al. 2007; Rowlinson et al. 2010, 2013, 2014; Fan et al. 2013a,b; Gompertz et al. 2013, 2014; Lü & Zhang 2014; Dall’Osso et al. 2015; Lü et al. 2015, 2018, 2019; Gao et al. 2016, 2017a,b; Lasky & Glampedakis 2016; Lasky et al. 2017; Ai et al. 2018, 2020; Lin & Lu 2019; Zou et al. 2019, 2021b; Lan et al. 2020a, 2021; Lin et al. 2020a; Sarin et al. 2020; Zhao et al. 2020; Ai & Zhang 2021; Xie et al. 2022a,b). However, as the GRB’s central engine, the newborn magnetar should be highly magnetized and rapidly rotating, due to the fact that it inherited prodigious angular momentum from its progenitor and undergone extreme magnetic field amplification during the progenitor’s catastrophic process. Thus, it is natural to consider that a fraction of the progenitor fragment in post-collapse or post-merger could not escape from the central magnetar and could circulate into an accretion disk and interact with a nascent magnetar, which could have a strong influence on the spin evolution and transient EM emission of newborn magnetar (namely, magnetic propeller model). To date, the propeller model has been widely used to explain some observations in GRBs and supernovae (SNe), such as the significant brightening early afterglows in some GRBs (Dai & Liu 2012; Li et al. 2021; Yang et al. 2024), the precursor emission and X-ray flares in LGRBs (Bernardini et al. 2013; Gibson et al. 2018; Lan et al. 2018; Yu et al. 2024), the extended emission and X-ray plateau emission in SGRBs (Gompertz et al. 2014; Gibson et al. 2017; Lan et al. 2020b), as well as some special SNe (Piro & Ott 2011; Lin et al. 2021). Meanwhile, such an interacting magnetar-disk system tends to reach an equilibrium spin state, where the equilibrium spin period ( $P_{\text{eq}}$ ) and surface magnetic field strength ( $B_p$ ) will follow a positive correlation for a given accretion rate, i.e.,  $B_p \propto P_{\text{eq}}^{7/6}$  (Piro & Ott 2011). Interestingly, such a correlation has been found in relevant statistical studies based on GRB and SN samples that are believed to be powered by the central magnetar (Stratta et al. 2018; Lin et al. 2020b; Xie et al. 2022a). Furthermore, Stratta et al. (2018) and Lin et al. (2020b) tentatively investigated the mass accretion rate of newborn accreting magnetar in the propeller model based on their respective GRB samples, and the corresponding mass accretion rates are inferred as  $\dot{M} \sim 10^{-4} - 10^{-1} M_{\odot} \text{ s}^{-1}$ . However, the accretion rates derived from the propeller model are highly dependent on the  $B_p$  and initial period ( $P_0$ ) obtained through X-ray plateau data, as well as the

gravitational mass ( $M_g$ ), radius ( $R$ ) and moment of inertia ( $I$ ) of the newborn magnetar, and their constraints on accretion rates typically assume fixed values for the mass, radius and moment of inertia of the newborn magnetar ( $M_g \sim 1.4M_\odot$ ,  $R \sim 10\text{km}$ ,  $I = 0.35M_gR^2$ ), which simplification may deviate from the true mass accretion rate of the newborn accreting magnetar. In particular, [Lan et al. \(2025\)](#) found that neglecting the  $R/I$  evolutionary effects can lead to systematic overestimation or underestimation of magnetar physical parameters such as  $B_p$  and  $P_0$  from 20% to 50%. The  $R/I$  evolutionary effects and different gravitational masses may significantly impact the accretion rate results obtained from the  $B_p - P_0$  distribution for newborn accreting magnetar.

It is interesting to ask the following two questions: What is the true mass accretion rate of newborn accreting magnetar after incorporating  $R/I$  evolutionary effects and different gravitational masses? What constraints can one pose on the progenitors in our LGRBs from the true mass accretion rates? In this paper, we systematically explore the propeller properties of accreting magnetar by utilizing an LGRB sample with X-ray plateau in [Lan et al. \(2025\)](#), and try to constrain the accretion rate of accreting magnetar in different EoSs and X-ray radiative efficiencies, which is crucial to helping us understand the nature and physical environment of newborn accreting magnetar and its progenitor. Our paper is organized as follows. The sample selection and data reduction are presented in Section 2. In Section 3, we briefly introduce the model of a magnetar propeller with fallback accretion. In Section 4, we show the  $B - P$  statistical results in different EoSs, and further constrain the accretion rate of accreting magnetar in different EoSs and X-ray radiative efficiencies. Finally, we summarize our conclusions and discussions in Section 5. Throughout the paper, a concordance cosmology (flat  $\Lambda$ CDM) with parameters  $H_0 = 67.4 \text{ km s}^{-1} \text{ Mpc}^{-1}$ ,  $\Omega_M = 0.315$ , and  $\Omega_\Lambda = 0.685$  has been adopted according to the *Planck* results ([Planck Collaboration et al. 2020](#)).

## 2. SAMPLE SELECTION AND DATA REDUCTION

Theoretically, the magnetar energy injection signature typically exhibits a shallow decay segment (or plateau), followed by a steeper decay segment in X-ray emission when it is spinning down. [Lan et al. \(2025\)](#) systematically searched for LGRBs with X-ray plateau emission by using all available *Swift* GRB catalog, which includes more than 1500 GRB outbursts between 2005 January and 2023 November. Finally, they found that 105 LGRBs were able to satisfy magnetar engine candidates, 43 of which have a measured redshift. We mainly used these 105 curated magnetar engine candidate samples to statistically study the propeller properties of LGRB remnant. It should be noted that the redshift measurement  $z$  is vital to derive the intrinsic luminosity parameter, and we adopted  $z = 1$  for the GRBs without the redshift measurement in our sample.

Once the sample has been determined, to investigate in-depth the physical properties of newborn magnetar, one should next estimate the physical parameters of these magnetars. However, the magnetar parameters inferred from the observed X-ray plateau data are strongly dependent on the X-ray radiative efficiency  $\eta_X$  and the  $R/I$  evolutionary effects. On the one hand,  $\eta_X$  is quite uncertain and could evolve over time. [Xiao & Dai \(2019\)](#) claimed that  $\eta_X$  is largely dependent on the bulk saturation Lorentz factors ( $\Gamma_{\text{sat}}$ ) of magnetar wind, and found that a typical value  $\Gamma_{\text{sat}} \sim 300$  in the GRBs corresponds to  $\eta_X$  possibly close to 0.01. [Zhong et al. \(2024\)](#) suggested that the radiative efficiency evolves with time during the magnetar spin-down process and estimated the time-averaged radiation efficiency as  $\sim 0.01$  for GRB 230307A. [Rowlinson et al. \(2014\)](#) suggested that the conversion efficiency of rotational energy from the magnetar wind to the observed X-ray plateau luminosity is  $\leq 0.2$ . [Gao et al. \(2016\)](#) found the efficiency parameter within 0.5 by Monte Carlo simulation. It is worth noting that in the framework of magnetar spin-down, a low radiation efficiency, such as  $\eta_X < 0.1$ , would lead to the magnetar rotational speed that breaks through the Keplerian break-up limit, which may challenge the current of most NS EoS models. Therefore, we took two radiation efficiency values to evaluate our results, i.e.  $\eta_X = 0.1, 0.5$ . On the other hand, [Lan et al. \(2025\)](#) found that neglecting the evolutionary effects of  $R/I$  can lead to systematic overestimation or underestimation of magnetar physical parameters such as  $B_p$ ,  $P_0$ , and ellipticity ( $\epsilon$ ) from 20% to 50%. Thus, when using the observed X-ray plateau data to analyze the properties of the newborn magnetar, we should simultaneously combine the EoS and  $\eta_X$  information as constraints to accurately estimate various parameters of the newborn magnetar.

We employed the Markov Chain Monte Carlo (MCMC) method from the emcee Python package ([Foreman-Mackey et al. 2013](#)) to derive the best-fitting posterior magnetar parameters and their uncertainties in 4 EoSs [SLy ([Douchin & Haensel 2001](#)), WFF2 ([Wiringa et al. 1988](#)), ENG ([Engvik et al. 1996](#)), AP3 ([Akmal & Pandharipande 1997](#))] with baryonic mass  $M_b = 2.0 M_\odot$  and two X-ray radiation efficiency ( $\eta_X = 0.1, 0.5$ ). The key physical parameters for defining the properties of a newborn magnetar are the initial spin period  $P_0$ , the dipole magnetic field strength  $B_p$ , and the deformed ellipticity  $\epsilon$ . The prior  $P_0$  was set within a uniform distribution over a broad range, and the prior  $B_p$  and

$\varepsilon$  were set within a log-uniform distribution over a broad range, specifically  $P_0/\text{ms} \in [0.3, 40]$ ,  $\log(B_p/\text{G}) \in [13, 16]$ , and  $\log \varepsilon \in [-6, -2]$ . Based on the value of  $\chi^2/\text{dof}$ , we determined the best-fitting model parameters for each GRB in different EoSs and X-ray radiation efficiencies. For more details on constraining magnetar parameters by taking into account the  $R/I$  evolutionary effects, please refer to our latest paper in Lan et al. (2025). Ultimately, we collected magnetar parameters ( $B_p$  and  $P_0$ ) in various combination situations by considering constraints from different EoSs and  $\eta_X$ .

### 3. MAGNETAR PROPELLER ACCRETION MODEL

The propeller model was first theoretically proposed by Illarionov & Sunyaev (1975) to elucidate the dynamical processes of how highly magnetized NS can lose angular momentum and regulate accretion when their magnetic fields interact with inflowing materials from the accretion disk. If the NS has a strong magnetic field ( $B_p \gtrsim 10^{12}$  G) and is rapidly rotating, as expected for the NSs in GRBs. In this case, the local materials of accretion disk could be threw by centrifugal force rather than accreted onto the NS. Finally, the interaction between a magnetar with its surrounding accretion disk has an effect on its spin evolution and hence the accretion outflows. This propeller accretion model has been widely discussed in the context of GRBs that are likely powered by magnetars (Dai & Liu 2012; Bernardini et al. 2013; Gompertz et al. 2014; Gibson et al. 2017, 2018; Lan et al. 2018, 2020b; Li et al. 2021; Lin et al. 2020b; Yang et al. 2024; Yu et al. 2024).

Within the propeller accretion model, the interaction between magnetar and its surrounding accretion disk can be modeled by defining the relative positions of Alfvén radius (the radius at which the dynamics of the gas within the disc is strongly influenced by the magnetic field,  $r_m$ ), corotation radius (the radius at which material in the disc orbits at the same rate as the magnetar surface,  $r_c$ ), and light cylinder radius (the radius at which the magnetic field lines rotate at the speed of light in order to maintain rigid rotation with the NS surface,  $r_{lc}$ ). The magnetic dipole field of the central magnetar is given by  $B = \mu/r^3$ , where  $\mu = B_p R^3$  is the magnetic dipole moment for a NS with surface dipole field  $B_p$  and radius  $R$ . The magnetic pressure at a given radius  $r$  can be expressed as

$$P_{\text{mag}} = \frac{B^2}{2\mu_0} = \frac{\mu^2}{2\mu_0 r^6}, \quad (1)$$

where  $\mu_0$  is the permeability in vacuum. There is also an inward ram pressure on the accreted material that falls back from the accretion disc, which competes with the  $P_{\text{mag}}$ . For the case of spherically symmetric accretion, the ram pressure can be given by

$$P_{\text{ram}} = \frac{\dot{M}}{8\pi} \left( \frac{2GM_g}{r^5} \right)^{1/2}, \quad (2)$$

where  $G$  is the gravitational constant,  $M_g$  and  $\dot{M}$  are the gravitational mass and the accretion rate of central magnetar, respectively. Equating these two pressures gives the radius at which the fallback material is strongly affected by the dipole magnetic field, known as the Alfvén radius  $r_m$ , which could be written as

$$r_m = \mu^{4/7} (GM_g)^{-1/7} \dot{M}^{-2/7}, \quad (3)$$

$r_m$  is one of the three key radii that determine the spin evolution behavior of central magnetar. The second key radius is the corotation radius  $r_c$ , which is the radius at which the material orbits at the same rate as the stellar surface. Given that inflowing materials rotate at the local Keplerian angular velocity, i.e.,  $\Omega_K = (GM_g/r^3)^{1/2}$ , their corotation angular velocity with the central magnetar occurs at a radius of

$$r_c = (GM_g/\Omega^2)^{1/3}, \quad (4)$$

where  $\Omega = 2\pi/P$  and  $P$  are the angular velocity and spin period of the central magnetar, respectively. Furthermore, another critical radius is the radius of the light cylinder  $r_{lc}$ , where the magnetic field lines will rotate at the speed of light to maintain a rigid rotation with the magnetar surface. Thus,  $r_{lc}$  is defined as

$$r_{lc} = c/\Omega, \quad (5)$$

The dynamical evolution process and the accretion outflow transport pathway of the magnetar-disk system are fundamentally dictated by the spatial hierarchy among  $r_m$ ,  $r_c$ , and  $r_{lc}$ . Specifically speaking, when  $r_m < r_c < r_{lc}$ , the

disk materials in the inner radius revolve faster than the magnetar, and the magnetic field will first slow the disk materials within  $r_c$ . Once the angular momentum of the materials is lost, the disk materials can no longer keep Keplerian rotation at the orbit and tend to accrete to the surface of the NS along the magnetic field lines, resulting in the spin-up of the magnetar, i.e., the so-called accretion regime. Conversely, if  $r_c < r_m \ll r_{lc}$ , the magnetic field is spinning faster than the inner disk materials, and materials already within  $r_c$  accrete to the surface of the magnetar, while the materials within the range of  $r_c$  and  $r_m$  will be accelerated to a super-Keplerian velocity and propelled away the system by the centrifugal force. The angular momentum of the magnetar is transferred to the inner disk materials and causes the spin-down of the magnetar, i.e., the so-called propeller regime. If the propeller power is not strong enough for the materials, it cannot reach the potential well. Then, the materials will return to the disc without any emission signals to be detected.

Notably, the relative positions of  $r_c$  and  $r_m$  always change dynamically in the accretion regime and the propeller regime. In the accretion regime, the magnetar is spun up by gaining angular momentum from accretion, and the increased spin velocity will cause  $r_c$  to shrink. Then, as the accretion rate decreases, the Alfvén radius  $r_m$  will expand until  $r_c < r_m$ , which will switch on the propeller regime. In the propeller regime, the magnetar is spun down by transferring angular momentum to the inner disk materials, and the decreased spin velocity will in turn cause  $r_c$  to expand. Once  $r_c > r_m$ , the system will switch on the accretion regime again. As we describe above, there would be several critical values for the accretion rate of such a magnetar-disk system. The magnetar spin-down rate due to the loss of angular momentum from a magnetized wind is enhanced when the Alfvén radius resides inside the light cylinder. This condition ( $r_m < r_{lc}$ ) is satisfied above a critical accretion rate of

$$\dot{M}_{lc} = \left(\frac{c}{2\pi}\right)^{-7/2} (GM_g)^{-1/2} B_p^2 R^6 P^{-7/2} (r_m = r_{lc}), \quad (6)$$

as  $r_m$  continues to shrink, the enhancement of the spin-down rate reaches saturation when  $r_m$  is pushed all the way down to the NS surface, a condition that requires an even higher accretion rate of

$$\dot{M}_{NS} = (GM_g)^{-1/2} B_p^2 R^{5/2} (r_m = R), \quad (7)$$

Obviously,  $\dot{M}_{NS}$  depends only on NS EoS and is independent of the rotation period. When  $R_{NS} < r_m < r_{lc}$ , whether the materials accrete freely onto the magnetar or whether the system may enter the more complicated propeller regime depends on the location of  $r_c$  relative to  $r_m$ . Ultimately, such a magnetar-disk system tends to evolve toward  $r_c \simeq r_m$  if the spin evolution of the magnetar is dominated by the interaction with its accretion disk. When  $r_c$  equals  $r_m$ , the accreting magnetar would reach an equilibrium spin period and accretion rate, which can be expressed as (Piro & Ott 2011)

$$\dot{M}_{eq} = (2\pi)^{7/3} (GM_g)^{-5/3} B_p^2 R^6 P_{eq}^{-7/3}, P_{eq} = 2\pi (GM_g)^{-5/7} B_p^{6/7} R^{18/7} \dot{M}_{eq}^{-3/7}, \quad (8)$$

Distinctly, the equilibrium spin period is independent of the initial spin period of newborn magnetar but correlates with the magnetic field strength, fallback accretion rate, gravitational mass and radius of the central magnetar. The gravitational mass and radius of neutron stars remain intrinsically tied to the poorly constrained EoS of matter at the nuclear density. Once the EoS and baryonic mass are given, one can infer the gravitational mass and radius of the neutron star by using the universal baryonic-to-gravitational mass conversion relation, combined with a numerical solution to the neutron star field equations. Therefore, the mass accretion rate can be quantitatively estimated via statistical analysis of the  $B_p$ - $P_0$  distribution in a population of accreting magnetars, where the equilibrium spin condition links the relation  $\dot{M} \propto B_p^2 P_{eq}^{-7/3}$ . Furthermore, assuming a constant mass accretion rate, the evolutionary timescale, before the newborn magnetar reaches such a spin equilibrium, can be estimated by (Metzger et al. 2018)

$$t_{ev} \simeq \frac{2\pi I / P_{eq}}{\dot{M} (GM_g r_m)^{1/2}} = (GM_g)^{2/7} I B_p^{-8/7} R^{-24/7} \dot{M}^{-3/7}, \quad (9)$$

where  $I = 0.35 M_g R^2$  is the moment of inertia. Obviously, the larger mass accretion rate and the stronger magnetic field correspond to a shorter timescale  $t_{ev}$ . For an accreting magnetar that has reached equilibrium period rotation, our estimate of  $t_{ev}$  can be considered as the lower limit for the accretion timescale ( $t_{acc}$ ).

In addition, the interaction between a magnetar and its surrounding accretion disk has an effect on its spin evolution. The energy reservoir of a newly born magnetar is the total rotational energy, which could be estimated as

$$E_{rot} = \frac{1}{2} I \Omega^2, \quad (10)$$

Typically, the rotation energy boundary is  $E_{\text{rot}} \simeq 3 \times 10^{52}$  ergs for an NS of gravitation mass  $1.4M_{\odot}$  rotating near the break-up period of  $P \simeq 1$  ms, but reservoirs up to  $E_{\text{rot}} \simeq 10^{53}$  ergs are possible for more massive NSs ( $M_{\text{g}} \gtrsim 2M_{\odot}$ ) with a stiff EoS (Metzger et al. 2015). In spin-down process, we consider that the rotational energy of newborn magnetar is mainly lost to a polar Poynting flux-dominated wind at a rate

$$\dot{E}_{\text{sd}} = \left( \frac{f_{\Phi}}{f_{\Phi, \text{lc}}} \right)^2 \frac{\mu^2 \Omega^4}{c^3}, \quad (11)$$

here we have assumed that the magnetic dipole moment and rotational axes are aligned. The  $f_{\Phi} = \int_0^{\theta_{\text{lc}}} \sin \theta d\theta \simeq \theta_{\text{lc}}^2/2$  is the fraction of the magnetar surface threaded by open magnetic flux, and  $\theta_{\text{lc}}$  is the latitude from the pole of the last closed field line (Bucciantini et al. 2006). For an isolated accreting magnetar, the closed field lines are typically assumed to extend to the light cylinder  $r_{\text{lc}}$ , corresponding to  $\theta_{\text{lc}} \simeq \sin^{-1}(R/r_{\text{lc}})^{1/2} \simeq (R/r_{\text{lc}})^{1/2}$  (Contopoulos et al. 1999; Spitkovsky 2006), thus providing a minimum open flux of  $f_{\Phi, \text{lc}} = R_{\text{NS}}/2r_{\text{lc}}$ . In this limit ( $f_{\Phi} = f_{\Phi, \text{lc}}$ ), one recovers from equation (11) the normal magnetic dipole spin-down rate  $\dot{E}_{\text{sd}} \propto \Omega^4$  of the force-free magnetar wind. By comparison, for an accreting magnetar with  $r_{\text{m}} \lesssim r_{\text{lc}}$ , closed field lines are truncated where the accretion disk begins, in which case  $\theta_{\text{lc}} \simeq (R/r_{\text{m}})^{1/2}$  and  $\dot{E}_{\text{sd}}$  is thus enhanced over the standard magnetic dipole rate by a factor of  $(r_{\text{m}}/r_{\text{lc}})^{1/2} > 1$  (Parfrey et al. 2016). The maximum spin-down rate is achieved for the maximum open flux  $f_{\Phi, \text{max}} \simeq 1$  at  $r_{\text{m}} = R$ , i.e., the limit of a split monopole spin-down. Combining above results, the magnetar wind energy loss rate of accreting magnetar is given by

$$\begin{aligned} \dot{E}_{\text{sd}} &\simeq \begin{cases} \frac{\mu^2 \Omega^4}{c^3} \frac{r_{\text{lc}}^2}{R^2}, & \dot{M} \gtrsim \dot{M}_{\text{NS}} \\ \frac{\mu^2 \Omega^4}{c^3} \frac{r_{\text{lc}}^2}{r_{\text{m}}^2}, & \dot{M}_{\text{lc}} \lesssim \dot{M} \lesssim \dot{M}_{\text{NS}} \\ \frac{\mu^2 \Omega^4}{c^3}, & \dot{M} \lesssim \dot{M}_{\text{lc}} \end{cases} \\ &\simeq \begin{cases} \frac{4\pi^2}{c} B_p^2 R^4 P^{-2}, & \dot{M} \gtrsim \dot{M}_{\text{NS}} \\ \frac{4\pi^2}{c} (GM_{\text{g}})^{2/7} (B_p R^3)^{6/7} P^{-2} \dot{M}^{4/7}, & \dot{M}_{\text{lc}} \lesssim \dot{M} \lesssim \dot{M}_{\text{NS}} \\ \frac{16\pi^4}{c^3} B_p^2 R^6 P^{-4}, & \dot{M} \lesssim \dot{M}_{\text{lc}} \end{cases} \end{aligned} \quad (12)$$

Combining equations (6), (7), (8) and (12), one can give the contours of various fixed spin-down powers, which can help us to infer the physical properties and energy mechanisms of the accretion magnetar.

#### 4. B-P STATISTICAL PROPERTIES AND ACCRETING MAGNETAR PROPERTIES

With the above MCMC method and the magnetar propeller accretion model, we can accurately estimate the physical parameters of the newborn magnetar and perform the  $B_p - P_0$  statistical analysis to constrain the accretion rate of accreting magnetar in different EoSs and  $\eta_{\text{X}}$  based on the 105 LGRBs with X-ray plateau emission that are thought to be fed by the central magnetar. As shown in Figure 1, putting (EoS,  $\eta_{\text{X}}$ ) all combinatorial results, we can find that the newborn magnetars of LGRBs in our sample with  $P_0 \sim 1$  ms usually possess  $B_p \sim 10^{13.5} - 10^{15}$  G, while those with  $P_0 \gtrsim 3$  ms are accompanied by a strong magnetic field of  $B_p \sim 10^{14.5} - 10^{15.5}$  G. Furthermore, we systematically investigated possible correlations between  $B_p$  and  $P_0$  of the newborn magnetar by applying a least-squares regression algorithm to all combinations of (EoS,  $\eta_{\text{X}}$ ).

In Figure 1, we show a series of  $B_p - P_0$  scatter distribution diagrams for all combinations of (EoS,  $\eta_{\text{X}}$ ). Interestingly, we found that there are generally strong correlations between  $B_p$  and  $P_0$  for all combinations of (EoS,  $\eta_{\text{X}}$ ). Most GRBs in our sample fall into the  $3\sigma$  deviation region of the best-fit power-law model. The  $B_p/P_0$  center values of Gaussian fit and the  $B_p - P_0$  best fit correlation results for various combinatorial scenarios are reported in Table 1. The strong correlations of  $B_p - P_0$  appeared to be universal for all combinations of (EoS,  $\eta_{\text{X}}$ ), which may indicate that the magnetic field of newborn magnetar is coupled to the initial spin period. More interestingly, if we put all EoSs together, the overall best-fit correlations of  $B_p - P_0$  can be approximately described as  $B_p \propto P_0^{1.30 \pm 0.16}$ , with the  $1\sigma$  deviation included. Such a correlation seems to hint that the initial spin period  $P_0$  estimated from X-ray plateau observations could deviate from that of the magnetar at birth, but strongly links to the equilibrium spin period when the accreting magnetar has reached equilibrium due to its interactions with the surrounding accretion disk, known as the magnetar propeller mechanism. In the context of magnetar propeller mechanism, the magnetic field and spin period of accreting magnetar satisfy power-law relation  $B_p \propto P_{\text{eq}}^{7/6}$  for a given mass accretion rate. According to equation (8), we can also use the statistical distribution  $B_p - P_0$  in a population of accreting magnetars to constrain the mass accretion rate in

the given gravitational mass and radius of newborn magnetar, which are highly dependent on EoS and baryon mass of NS and can be inferred by using the universal baryonic-to-gravitational mass conversion relation, combined with a numerical solution to the neutron star field equations.

In NS problems, two masses are widely discussed, i.e. the baryonic mass  $M_b$  and the gravitational mass  $M_g$ . The former ( $M_b$ ) refers to the total mass of all the baryons (e.g. proton, neutron, etc.) that make up a neutron star when they are not gravitationally bound, and is theoretically relevant because it is directly connected to the initial mass of the iron core of the progenitor massive star, which undergoes gravitational collapse to form the neutron star. On the other hand, the latter ( $M_g$ ) refers to the mass measured directly from observations, and is smaller than  $M_b$  due to the subtraction of the nuclear binding energy. Studying the conversion relationship between  $M_b$  and  $M_g$  is crucial to set interesting lower limits on the maximum mass ( $M_{\text{TOV}}$ ) of non-rotating NS for ruling out some soft EoS models, and can accurately constrain the mass accretion rate of nascent magnetar at different EoSs and baryon masses. Gao et al. (2020) investigated the transformational relations between  $M_b$  and  $M_g$  for a non-rotating NS or a rotating NS, and found that the transformation of the baryonic mass to gravitational mass is universal approximated using the EoS-independent quadratic formula to all selected EoSs

$$M_b = M_g + A \times M_g^2, \quad (13)$$

where  $A$  is usually adopted as a constant number that depends on the EoS and spin period. Putting together the ( $M_b$ ,  $M_g$ ) results for all adopted EoSs, Gao et al. (2020) found that the overall best-fit  $A$  value is 0.080 for non-rotating NS only and 0.073 when different spin periods are considered. In this work, in order to precisely estimate the mass accretion rate of newborn magnetar at different EoSs and baryon masses. We need to use the statistical distribution  $B_p - P_0$  in a population of accreting magnetar and to know the gravitational mass and radius of the neutron star in different EoSs and spin periods. Based on the best fit Gaussian distribution center values  $P_0$  for our sample of newborn magnetar under various scenarios, combined with the  $M_b - M_g$  transition relation and public code RNS (Stergioulas & Friedman 1995) to solve the field equations for rotating NS, we can infer the corresponding gravitational masses and radii of newborn magnetar in various combinations of (EoS,  $M_b$ ,  $\eta_X$ ) for different spin periods  $P_0$ . The details are as follows: 1) According to Table 1 to get the central values  $P_0$  of the spin period distribution in various (EoS,  $M_b$ ,  $\eta_X$ ) combinations; 2) By numerically solving the field equations for rotating NSs using the public RNS code (Stergioulas & Friedman 1995), we can obtain the Keplerian periods  $P_k$  and the corresponding radii at  $P_0$  for various (EoS,  $M_b$ ,  $\eta_X$ ) combinations; 3) To estimate the  $P_k$  and  $P_0$  relations in various (EoS,  $M_b$ ,  $\eta_X$ ) combinations, and to determine the  $A$  values by searching for the best-fit results for the  $M_b - M_g$  conversion of rotating neutron stars in Table 2 of Gao et al. (2020), and then use the universal relation  $M_b = M_g + A \times M_g^2$  to obtain the corresponding  $M_g$  in various (EoS,  $M_b$ ,  $\eta_X$ ) combinations; 4) Finally, the ranges of mass accretion rate for newborn magnetar in various (EoS,  $M_b$ ,  $\eta_X$ ) scenarios are accurately estimated from Equation (8) and the  $B_p - P_0$  distribution in our GRB sample. Table 2 reported the characteristic parameters and the corresponding mass accretion rate for various (EoS,  $\eta_X$ ) combinations under the  $M_b = 2.0M_\odot$  scenario.

According to the results of Figure 1 and Table 2, in the context of the magnetar propeller mechanism, we can find that all our LGRB data in the  $B_p - P_0$  plane are encompassed by two lines corresponding to the range of mass accretion rates  $10^{-5} M_\odot \text{ s}^{-1} < \dot{M} < 10^{-2} M_\odot \text{ s}^{-1}$  in combining the results of (EoS,  $\eta_X$ ) together. The results are inconsistent with the statistical results in Stratta et al. (2018) and Lin et al. (2020b) that are in the range  $10^{-4} M_\odot \text{ s}^{-1} < \dot{M} < 10^{-1} M_\odot \text{ s}^{-1}$ , which used the constant  $R$ ,  $I$  and  $M_g$  ( $M_g = 1.4M_\odot$ ,  $R = 12 \text{ km}$ ,  $I = 0.35M_g R^2$ ) for their GRB sample, and the results for our constrained accretion rate are one order of magnitude lower compared to their results. A lower accretion rate appears to be more physically justified, since under a high accretion rate  $0.1M_\odot \text{ s}^{-1}$ , the mass accreted onto the surface of the magnetar could exceed  $1M_\odot$  before reaching the equilibrium spin period. This would likely cause the magnetar to collapse into a BH before attaining spin equilibrium, rendering the magnetar propeller mechanism ineffective. The main reason for this discrepancy should be that we have corrected the magnetar parameters  $B_p$  and  $P_0$  by systematically incorporating  $R/I$  evolutionary effects, and then using the  $M_b - M_g$  transition relation and the  $B_p - P_0$  statistical distributions of different EoSs and X-ray radiative efficiencies in combination with the propeller model. In other words, the propeller properties of accreting magnetar are obtained by using the constant  $R/I$  scenario in previous studies which will present results with a higher mass accretion rate, which may impair our understanding of the physical nature and its surroundings of accreting magnetar, and will further diminish the reliability of inverse inference about the physical properties of its progenitor. The precise constraint on

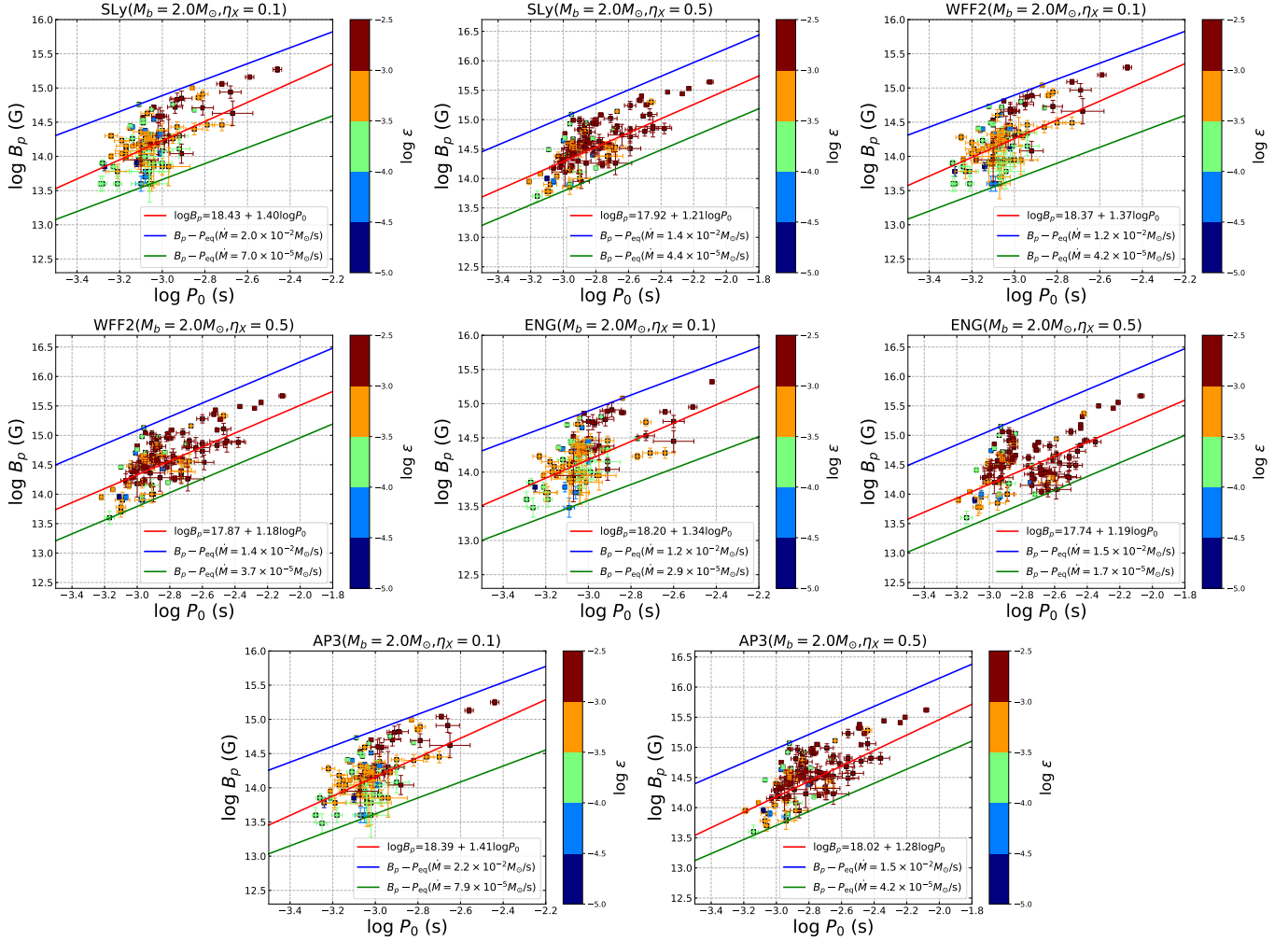


**Figure 1.** The distributions between the  $B_p$  and  $P_0$  for our LGRB sample in four EoSs with  $M_b = 2.0M_\odot$  and  $\eta_X = 0.1, 0.5$ . The different colors of these circular points correspond to different  $\epsilon$  values. The red solid lines show the best-fitting results, and green solid lines and blue solid lines represent the expected  $B_p - P_{eq}$  correlations at the lower and upper limits of the accretion rate derived from our LGRB sample.

the mass accretion rate utilizing evolved  $R/I$  will be crucial to understanding the physical nature of accreting magnetar and its progenitor.

Furthermore, we performed the relevant statistical analysis for the mass accretion rate in our GRB sample. In Figure 2, we show the probability density distributions and the cumulative distributions of mass accretion rate in different NS EoSs and radiative efficiencies. The log-normal distributions can be described as  $\log \dot{M}^{(\text{SLy}, \eta_X=0.1)}/M_\odot \text{ s}^{-1} = -3.02 \pm 0.56$ ,  $\log \dot{M}^{(\text{SLy}, \eta_X=0.5)}/M_\odot \text{ s}^{-1} = -3.10 \pm 0.56$ ,  $\log \dot{M}^{(\text{WFF2}, \eta_X=0.1)}/M_\odot \text{ s}^{-1} = -3.03 \pm 0.55$ ,  $\log \dot{M}^{(\text{WFF2}, \eta_X=0.5)}/M_\odot \text{ s}^{-1} = -3.11 \pm 0.57$ ,  $\log \dot{M}^{(\text{ENG}, \eta_X=0.1)}/M_\odot \text{ s}^{-1} = -3.04 \pm 0.59$ ,  $\log \dot{M}^{(\text{ENG}, \eta_X=0.5)}/M_\odot \text{ s}^{-1} = -3.30 \pm 0.70$ ,  $\log \dot{M}^{(\text{AP3}, \eta_X=0.1)}/M_\odot \text{ s}^{-1} = -2.97 \pm 0.56$ ,  $\log \dot{M}^{(\text{AP3}, \eta_X=0.5)}/M_\odot \text{ s}^{-1} = -3.06 \pm 0.57$ . To compare whether there are significant differences in the constrained mass accretion rates for different EoSs and radiative efficiencies, we used the Kolmogorov-Smirnov (K-S) algorithm to test the deviations of data set for different EoSs and radiative efficiencies. Putting  $\eta_X$  results for our adopted EoSs together, the overall  $p$ -value of the K-S test for the derived mass accretion rates between different NS EoSs and different radiative efficiencies can be approximately expressed as  $p_{\text{KS}} < 7.3 \times 10^{-1}$ ,  $p_{\text{KS}} < 5.3 \times 10^{-2}$ , respectively. The K-S test results indicate that the null hypothesis that the mass accretion rate sets of different EoSs and radiative efficiencies scenarios come from the same population cannot be rejected. Combining the results of Figure 2 and the K-S test, we can find that there are no significant differences in the constrained mass accretion rates for different EoSs, and the constraints on magnitude of mass accretion rate seem to be independent of the EoS stiffness. However, there are systematic differences in the

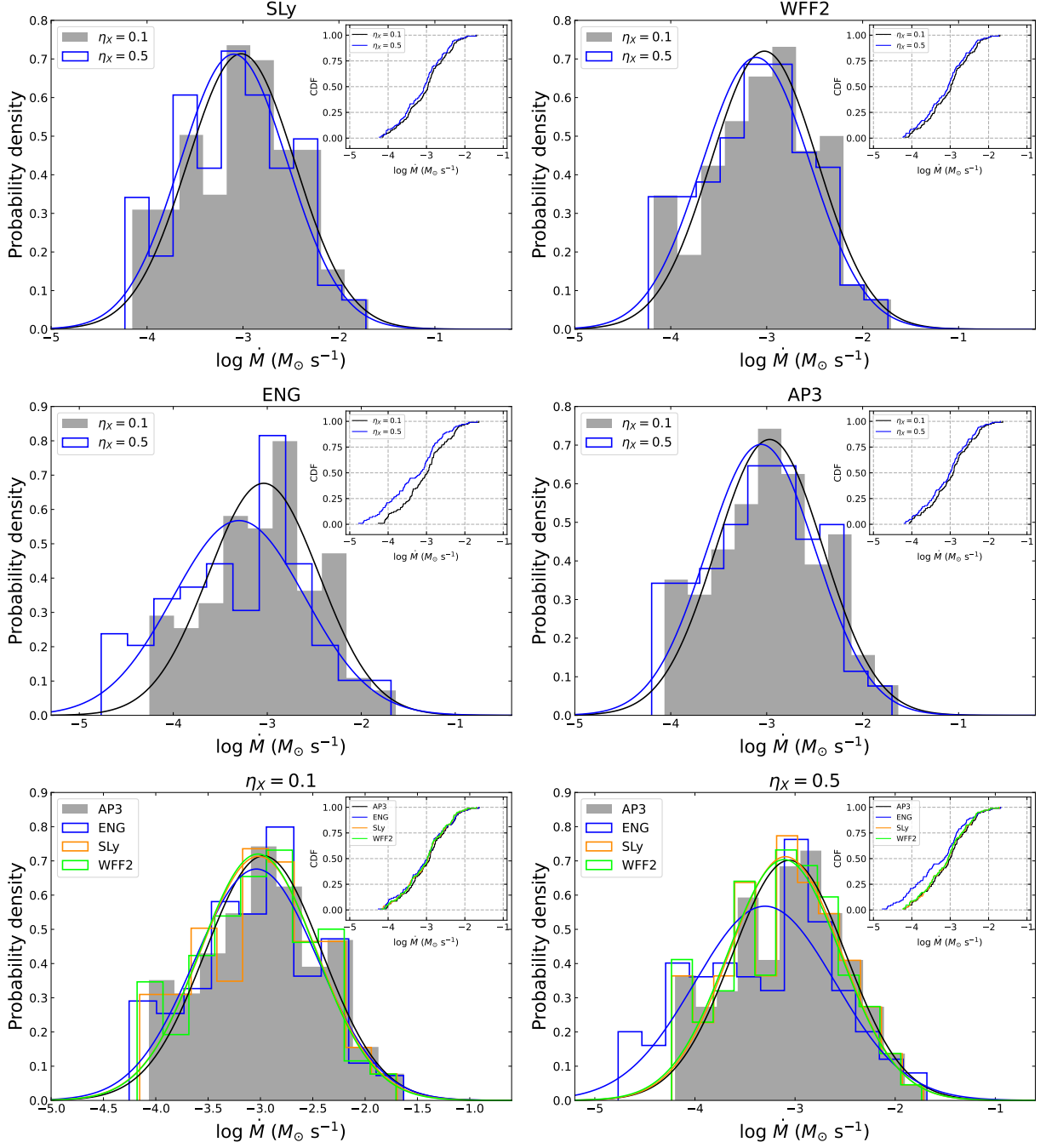


**Figure 2.** Comparisons of the derived magnetar accretion rate parameter  $\dot{M}$  histograms in different EoSs and  $\eta_X$  for our LGRB sample. The solid lines of different colors are the best Gaussian fits. The cumulative distributions corresponding to  $\dot{M}$  in different EoSs and  $\eta_X$  are also displayed in the inset.

constrained mass accretion rates for different radiative efficiencies, and with higher X-ray radiative efficiency, the constrained mass accretion rates tend to become larger.

It is important to note that the newborn magnetar is likely to collapse into a BH if it accretes a significant amount of materials and exceeds the maximum gravitational mass ( $M_{\text{max}}$ ) of a stable NS. One interesting question is: can the newborn accreting magnetars in our GRB sample have collapsed into BH before reaching the equilibrium spin period due to accreting a significant amount of materials and exceeding the maximum gravitational mass of NS? The collapse process would directly affect the sustainability of the magnetar central engine and the jet energy injection mechanism.

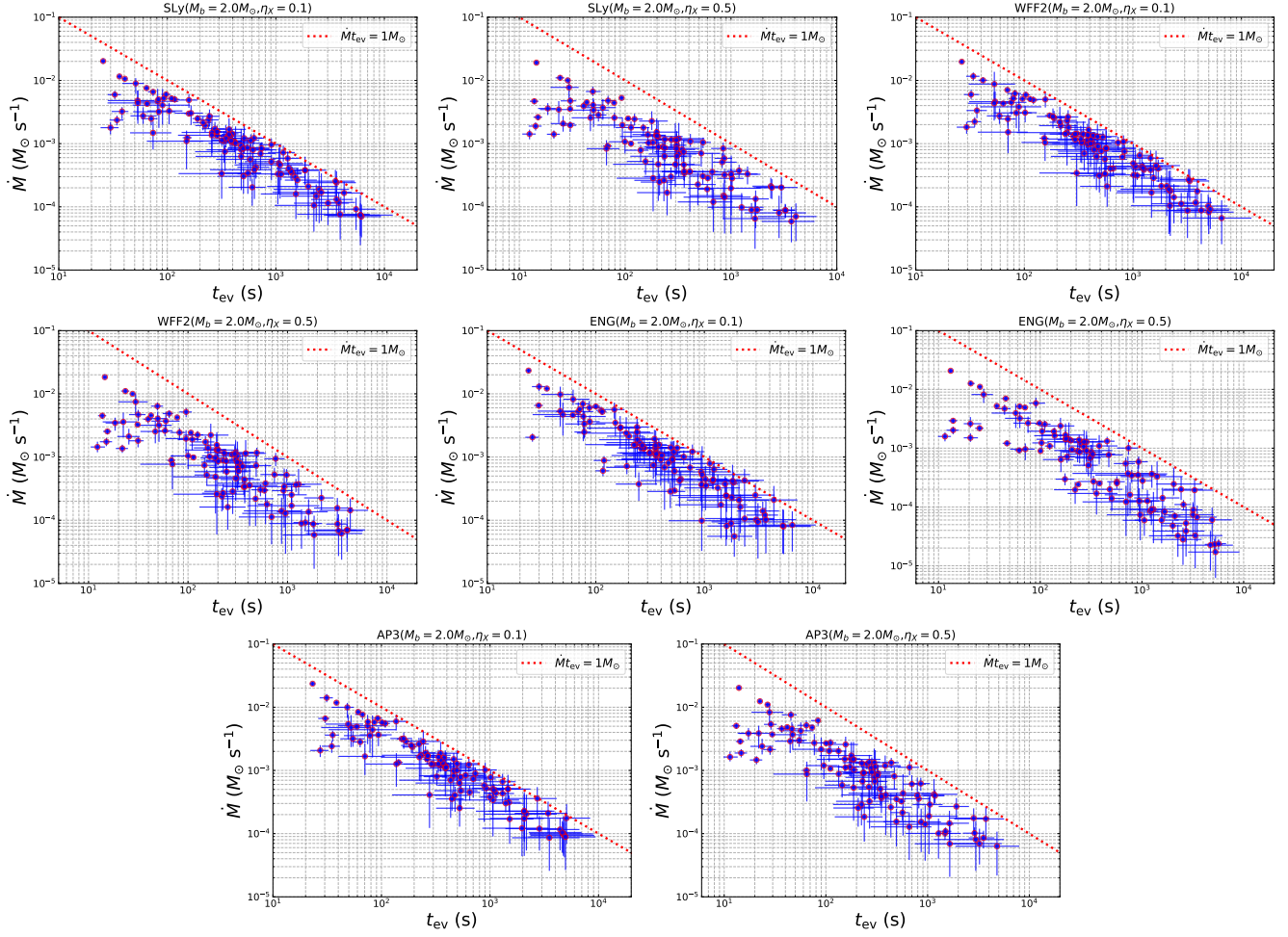


**Figure 3.** The accretion rate  $\dot{M}$  vs. the lower limit of accretion timescale  $t_{\text{ev}}$  in different EoSs and  $\eta_X$  for our LGRB sample. The red dotted lines corresponds to  $\dot{M} t_{\text{ev}} = 1 M_\odot$ .

Under certain approximations, we can try to estimate the accretion mass of newborn accreting magnetars in our GRB sample at reaching the equilibrium spin period. According to Equation (9), we first estimated the evolutionary timescales  $t_{\text{ev}}$  for these accreting magnetars to reach equilibrium spin period in various (EoS,  $\eta_X$ ) combination scenarios. In Figure 3, we plotted a series of  $\dot{M} - t_{\text{ev}}$  scatter diagrams for different EoSs and radiative efficiencies based on our GRB sample. We could find that the accretion masses of all newborn accreting magnetars and most newborn accreting magnetars in our GRB sample are less than  $1 M_\odot$  and  $0.5 M_\odot$  for various (EoS,  $\eta_X$ ) combination scenarios, respectively. Such statistical results seem to imply that the most newborn accreting magnetars in our GRB sample will not exceed the maximum gravitational mass of NS with stiff EoS before reaching the accretion equilibrium spin period, and will not collapse into BH before reaching the accretion equilibrium spin period for a NS with stiff EoS. In order to test whether these accreting magnetars in our GRB sample can actually survive the equilibrium spin period for our selected EoSs, we need to further estimate the maximum gravitational mass  $M_{\text{max}}$  and the total gravitational mass ( $M_{\text{tot}}$ ) of accreting NS for our selected EoSs.

For a given EoS, the maximum gravitational mass  $M_{\text{max}}$  of rotating NS depends on the rotation period and the maximum mass of non-rotating NS. It can be expressed as (Lyford et al. 2003; Lasky et al. 2014)

$$M_{\text{max}} = M_{\text{TOV}} (1 + \alpha P^\beta) \quad (14)$$

where  $\alpha$  and  $\beta$  depend on NS EoS, and the values of  $\alpha$  and  $\beta$  for our selected EoSs are presented in Table 2. For an accreting magnetar, the total gravitational mass energy when it reaches the accretion equilibrium spin period can be

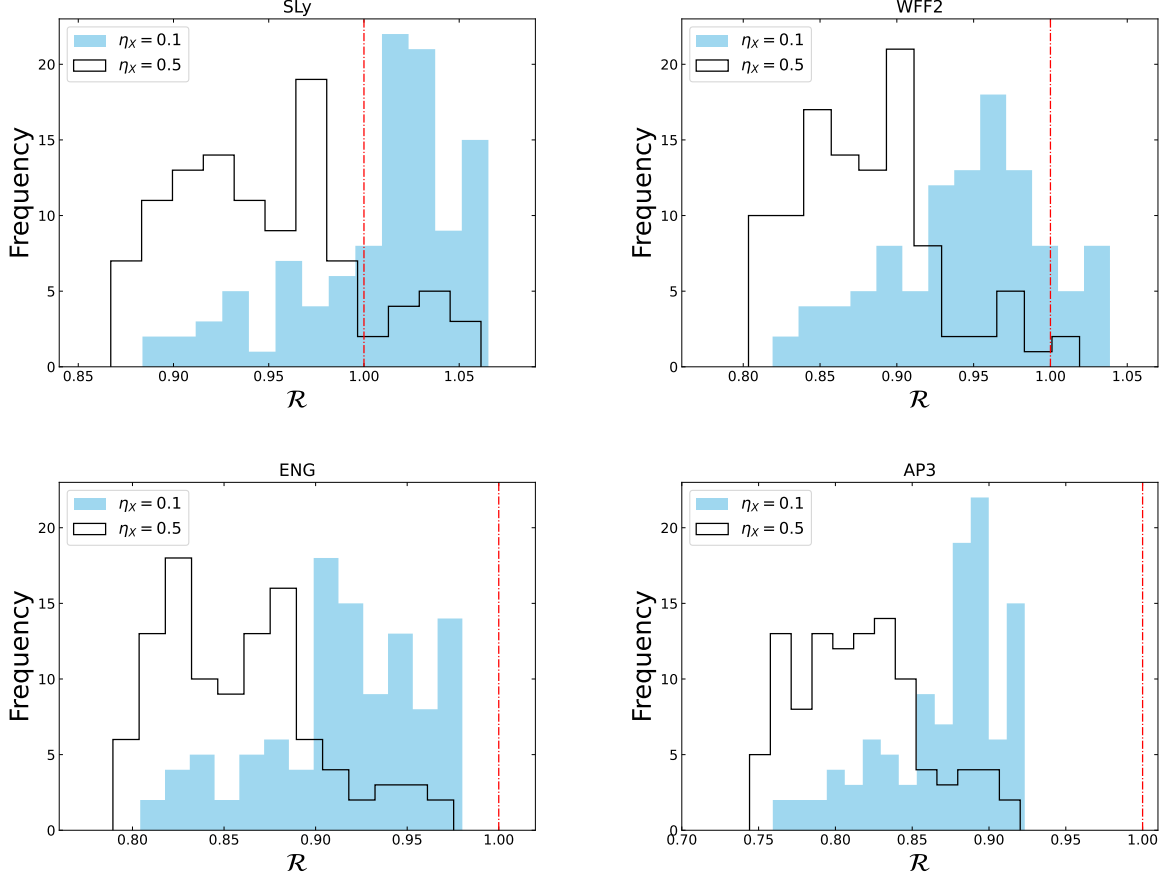


**Figure 4.** The distributions of the mass ratio parameter  $\mathcal{R} = M_{\text{tot}}/M_{\text{max}}$  in different EoSs and  $\eta_X$  for our LGRB sample. The red vertical dashed-dotted lines correspond to  $\mathcal{R} = 1$ , which marks the boundary where an accreting magnetar collapses into a BH.

expressed as

$$M_{\text{tot}} = M_g + M_{\text{acc}} \quad (15)$$

where  $M_{\text{acc}} \simeq \dot{M}_{\text{eq}} t_{\text{ev}}$  approximately represents the mass accreted onto the magnetar surface before reaching accretion equilibrium in the interacting magnetar-disk system. In order to identify whether the accreting magnetar has collapsed into a BH before reaching accretion equilibrium, we define a dimensionless mass ratio parameter  $\mathcal{R} = M_{\text{tot}}/M_{\text{max}}$ . If  $\mathcal{R} > 1$  is satisfied for the newborn accreting magnetar, we can assume that it has collapsed into a BH before it reaches the accretion equilibrium spin period. If  $\mathcal{R} < 1$  is satisfied for the newborn accreting magnetar, we can assume that it remains a stable NS when it reaches the accretion equilibrium spin period and will not collapse into a BH. Combining Equations (14) and (15), we can derive the distributions of mass ratio  $\mathcal{R}$  for our GRB accreting magnetar sample in various (EoS,  $\eta_X$ ) combination scenarios. In Figure 4, we show the distributions of mass ratio  $\mathcal{R}$  for our GRB accreting magnetar sample in different EoSs and radiative efficiencies. We can find that no matter whether the radiative efficiency  $\eta_X$  is 0.1 or 0.5, most of the accreting magnetars in our GRB sample can actually survive the equilibrium spin period for two soft SLy and WFF2 EoSs ( $M_{\text{TOV}} = 2.05M_{\odot}$ ,  $2.20M_{\odot}$ ), and all the accreting magnetars in our GRB sample can actually survive the equilibrium spin period for two stiff EoSs ( $M_{\text{TOV}} = 2.24M_{\odot}$ ,  $2.39M_{\odot}$ ). In other words, for various (EoS,  $\eta_X$ ) combination scenarios, the majority of the nascent accreting magnetars in our GRB sample are able to survive until they reach the equilibrium spin period, and will not collapse into black holes because their total mass after accreting materials to the magnetar surface does not exceed its maximum gravitational mass.

Further, we can try to infer the physical nature of the progenitors of accreting magnetar in our GRB sample under certain approximations. As the central engine of LGRBs with X-ray plateau emission, the newborn magnetar should be born in SN explosion and be highly magnetized and rapidly rotating. Thus, it is natural to consider that a fraction of the progenitor fragment in post-collapse could fall back to circulate into an accretion disk around the newborn magnetar with an accretion rate greatly exceeding the Eddington limit ( $\dot{M}_{\text{Edd}}$ ). The highly super-Eddington accretion disk is expected to generate a geometrically very thick, advection-dominated accretion disk (Beloborodov 1998), which likely drives large-scale outflows within the time range of our interest ( $\gtrsim 1000$  s since SN explosion; Dexter & Kasen 2013). Assuming that the accretion rate at the outer radius of the disk is equal to the mass fallback rate (Michel 1988; Metzger et al. 2018; Xu & Li 2019), we can derive the following formula

$$\dot{M}_{\text{d,out}} = \dot{M}_{\text{fb}} = \frac{2M_{\text{fb}}}{3t_{\text{fb}}} (1 + t/t_{\text{fb}})^{-5/3}, \quad (16)$$

where  $M_{\text{fb}}$  is the total fallback mass available for the accretion disk.  $t_{\text{fb}} = \epsilon t_{\nu}$  is the fallback timescale, and  $t_{\nu}$  and  $\epsilon$  are the viscous timescale and the ratio between the fallback timescale and the viscous timescale, respectively. Due to the fact that the fallback accretion process is often accompanied by mass outflow, only a fraction ( $\eta_1$ ) of the accretion rate would reach the inner disk radius, which is the true accretion rate onto the magnetar surface and can be expressed as

$$\dot{M}_{\text{d,in}} = \eta_1 \dot{M}_{\text{d,out}}, \quad (17)$$

where  $\eta_1$  is a dimensionless efficiency value with  $0 < \eta_1 < 1$ . Considering the effects of advection-dominated process and mass outflow, Mushtukov et al. (2019) found  $\eta_1 \gtrsim 0.6$  or  $\eta_1 \gtrsim 0.4$  when the disk outflow is powered by half or all of the viscously dissipated energy. Their numerical simulations also show that  $\eta_1$  will tend to approach the minimum as the initial accretion rate increases from 1 to  $\sim 1000 \dot{M}_{\text{Edd}}$ , which is significantly lower than our derived accretion rate for newborn magnetar in various (EoS,  $\eta_X$ ) combination scenarios. It is therefore a reasonable approximation to take  $\eta_1 = 0.8$  after ignoring the possible effect of chemical composition of the disk. In the context of the magnetar propeller model, the evolution of the accretion disk mass can be expressed as

$$\dot{M}_{\text{d}} = \dot{M}_{\text{fb}} - \dot{M}_{\text{prop}} - \dot{M}_{\text{acc}} \quad (18)$$

where  $\dot{M}_{\text{prop}}$  is the mass lost through the propeller mechanism, and  $\dot{M}_{\text{acc}} \simeq \dot{M}_{\text{d,in}}$  is the mass lost through the accretion onto the magnetar surface. Based on the description of Gibson et al. (2017),  $\dot{M}_{\text{prop}}$  and  $\dot{M}_{\text{acc}}$  can be defined as follows,

$$\dot{M}_{\text{prop}} = \eta_2 \left( \frac{M_{\text{d}}}{t_{\nu}} \right), \quad (19)$$

$$\dot{M}_{\text{acc}} = (1 - \eta_2) \left( \frac{M_{\text{d}}}{t_{\nu}} \right), \quad (20)$$

where  $\eta_2$  is the efficiency of the magnetar propeller mechanism. Gibson et al. (2018) and Yu et al. (2024) used the magnetar propeller accretion model to fit the X-ray data in their respective LGRB samples, and found that the magnetar propeller mechanism is highly efficient, with the propeller efficiency reaching  $\sim 0.8$  for most LGRBs in their sample. Therefore, it is a reasonable approximation to take  $\eta_2 = 0.8$  for our LGRB sample. When the material in the accretion disk is depleted, the propeller mechanism will no longer be effective. This indicates that all materials falling back to the disk are ultimately either accreted or thrown by the propeller after ignoring the possible effect of chemical composition of the disk. If we take the equilibrium spin period timescale  $t_{\text{ev}}$  as the lower limit of the accretion timescale  $t_{\text{acc}}$ , based on equations (8), (16), (17), (18), (19) and (20), one can express the lower limit of the fallback time scale  $t_{\text{fb}}$  as

$$t_{\text{fb}} \simeq 4t_{\text{ev}} \simeq 4(GM_g)^{2/7} I B_p^{-8/7} R^{-24/7} \dot{M}^{-3/7}, \quad (21)$$

Based on the above equations, we can estimate that the fallback rate of progenitor envelope materials onto the magnetar accretion disk in our LGRB sample can reach a range of  $\dot{M}_{\text{fb}} \simeq 2\dot{M}_{\text{acc}} \sim 10^{-5} - 10^{-2} M_{\odot} \text{ s}^{-1}$  at fallback times ranging

from  $t_{\text{fb}} \sim 20 - 10^4$  s for various (EoS,  $\eta_{\text{X}}$ ) combinations. Such an accretion timescale seems consistent with the fallback timescale derived for Wolf-Rayet (WR) star, i.e.  $\sim 10^2 - 10^5$  s<sup>1</sup>. For a shorter timescale, the fallback materials could come from the core of the progenitors, which suggests an origin of compact progenitor stars for some LGRBs (Campana et al. 2006; Woosley & Heger 2006). Next, we try to test whether the progenitor of the LGRBs in our sample can provide enough envelope materials to satisfy the accretion of newborn magnetar.

Consider an axisymmetric rotating star at the onset of core collapse. For simplicity, let us ignore the pressure forces and take the trajectory of each particle to correspond to free fall. Assuming that the progenitor star in our LGRBs is symmetric about its rotation axis and mirror-symmetric across the equator, when a particle (Particle 1) falls back from its initial position to the equatorial plane, it will collide with another particle (Particle 2) with a velocity of  $-v_z$  in the equatorial plane. The positions of the two particles are mirror-symmetric across the equator; see Figure 1 in Kumar et al. (2008). The time it takes for a particle at the initial position  $(r, \theta, \phi)$  with angular velocity  $\Omega(r, \theta)$  to fall back to the equatorial plane of the progenitor star at the end of its evolution trajectory is approximately (Kumar et al. 2008; Zhao et al. 2025)

$$t_{\text{eq}} \approx t_s(r) + \frac{\pi}{2^{3/2}\Omega_k} \left[ 1 + \frac{3}{4} \left( \frac{\Omega \sin \theta}{\Omega_k} \right)^2 \right], \quad (22)$$

where  $\Omega_k$  is the local Kepler angular velocity of the particle,  $t_s(r)$  is the sound propagation time from the center of the progenitor star to the initial position  $r$  of the particle, which is roughly the time it takes (from the start of collapse at the center) for gas at  $r$  to realize the loss of pressure support and begin its fall toward the center of the progenitor star.

We assume that the difference between the polar and equatorial radii of an equal-collapse-time surface is  $\delta r$ . For a fixed  $t_{\text{eq}}$ , the radial difference between particles that start at  $\theta = 0$  and those that start at  $\theta = \pi/2$  is (Kumar et al. 2008; Zhao et al. 2025)

$$\delta r \approx \frac{3\pi}{2^{7/2}} \frac{[\Omega(r)/\Omega_k(r)]^2}{\Omega_k(r) d(t_s + \pi 2^{-3/2} \Omega_k^{-1})/dr}, \quad (23)$$

Introducing the notation

$$H_t^{-1} \equiv \left| \frac{d}{dr} \ln[t_s + \pi 2^{-3/2} \Omega_k^{-1}] \right|, \quad (24)$$

combining equations (23) and (24), one can obtain

$$\delta r \sim \frac{H_t}{2} \left[ \frac{\Omega(r)}{\Omega_k(r)} \right]^2, \quad (25)$$

In the above equations, we have assumed  $t_s \sim \Omega_k^{-1}$ , which is valid outside a relatively small core region. Since  $\delta r \ll r$ , one can approximate the surface in equal-collapse-time as a sphere, and the mass fallback rate of materials on the equatorial plane of the progenitor star should be equal to the mass loss rate of the progenitor star per unit time (Kumar et al. 2008; Zhao et al. 2025)

$$\dot{M}_{\text{eq,fb}}(t_{\text{eq}}) \approx \frac{dM(r)}{dr} \frac{dr}{dt_{\text{eq}}} \approx \frac{4\pi r^2 \rho(r) H_t}{t_{\text{eq}}} \approx \frac{4\pi r^2 \rho(r)}{t_{\text{eq}} |d \ln \Omega_k/dr|}, \quad (26)$$

The formula shows that  $M_{\text{eq,fb}}$  is insensitive to the rotation profile in the progenitor star. However, the fallback radius where the stellar matter circularizes has a strong dependence on the angular velocity  $\Omega$ . After fallback to the equatorial plane of a progenitor star, the velocity of the materials can be decomposed into an azimuth  $\phi$  component around the equatorial plane and a radial  $r$  component toward the center. The velocity components in the two directions satisfy  $|v_r| > v_\phi$ , where the sign of  $v_r$  is negative and independent of the initial position of the particle. This will cause

<sup>1</sup> The radii ( $r_e$ ) of the envelopes of WR stars are  $\sim 10^{10} - 10^{12}$  cm (Koesterke & Hamann 1995). The free-fall timescale of the extended envelopes can be estimated by  $t_{\text{ff}} \sim (r_e^3/GM)^{1/2}$ , i.e.  $10^2 \lesssim t_{\text{ff}} \lesssim 10^5$  s.

the initial disk formed during the core collapse process to shrink rapidly toward the center, ending when it reaches a radius defined as the fallback radius  $r_{\text{fb}}$

$$r_{\text{fb}} \approx r \left( \frac{\Omega}{\Omega_k} \right)^2, \quad (27)$$

At the fallback radius, the specific angular momentum of the inflowing materials is equal to that of the local circular orbit. For our selected LGRBs with X-ray plateau emission, their progenitor stars should have a core-envelope structure, as is common in stellar models. At the end of the progenitor star's life, most of the mass in its core part collapses into a rapidly spinning NS, a fraction of the progenitor fragment in post-collapse could circulate into an accretion disk and interact with the newborn magnetar. Such an interacting magnetar-disk system will undergo the accretion regime and propeller regime to accrete material onto the magnetar's surface and throw material away system, which would have a strong influence on the spin evolution and transient EM emission of the newborn magnetar. It should be noted that the shrink timescale for the initial accretion disk is much shorter than  $t_{\text{eq}}$ . Thus, we can equate the fallback rate of materials onto the accretion disk with the fallback rate of materials onto the equatorial plane, i.e.,  $\dot{M}_{\text{eq,fb}} = \dot{M}_{\text{fb}}$ . Assuming that the formation time of the newborn NS is  $t_{\text{NS}}$ , and given the density and spin profiles of the progenitor, we can obtain the fallback rate  $\dot{M}_{\text{fb}}(t)$  of the star's material on the accretion disk for  $t = t_{\text{eq}} - t_{\text{NS}}$ .

Based on the above equations, once we know the density profile and spin profile of the progenitor star, we can numerically solve for the fallback accretion rate at any given time. Liu et al. (2018) provided the density profiles of the progenitor star with different metallicities and masses, and Kumar et al. (2008) gave the spin profile of the progenitor star. We thus calculated the evolution of the fallback rate for various progenitor materials with different metallicities and masses on the accretion disk. To ensure that the residual remnant is an NS, we selected only progenitor stars with masses below  $25M_{\odot}$  for the numerical solution. As shown in Figure 5, we can find that the fallback rate of progenitor envelope materials onto the magnetar accretion disk for our LGRB sample in various (EoS,  $\eta_X$ ) combination scenarios is compatible with the theoretical mass fallback rate of some low-metallicity massive progenitor stars such as those with  $(Z \lesssim 10^{-2}Z_{\odot}, M \gtrsim 26M_{\odot})$ ,  $(Z \lesssim 10^{-2}Z_{\odot}, M \gtrsim 20M_{\odot})$ ,  $(Z \lesssim 10^{-4}Z_{\odot}, M \gtrsim 15M_{\odot})$ , and so on. These results suggest that the low-metallicity progenitors can provide enough material to satisfy the accretion requirements of the newborn accreting magnetar in our LGRB sample for various (EoS,  $\eta_X$ ) combination scenarios. The solar metallicity stars might not be so available to serve as the progenitors for our LGRB sample.

Ultimately, we investigated the spin-down evolution regimes of newborn magnetar for parameter space of the mass accretion rate  $\dot{M}$  and the spin period  $P_0$  in different EoSs and  $\eta_X$ , and examined the positions of our LGRB sample within the parameter space of  $\dot{M}$  and  $P_0$ , as well as tried to test whether the rotational energy of this newly formed accreting magnetar could sustain the energy required for the propeller model radiation for our LGRB sample in various (EoS,  $\eta_X$ ) combinations. Based on equations (6), (7), (8), and (12), we can infer the magnetar spin-down power contours in the propeller mechanism and test the energy required for the magnetar spin-down and propeller model radiation for our LGRB sample in various EoSs and  $\eta_X$ . In Figure 6, we show a series of  $\dot{M} - P_0$  scatter diagrams in various (EoS,  $\eta_X$ ) combinations. As shown in Figure 6, we can find that all GRBs in our sample fall well within the region where the EM dipole radiation and the propeller mechanism jointly modulate the spin evolution of newborn magnetar, and the overall requirement for energy release  $\dot{E}_{\text{sd}} \subseteq (10^{49}, 10^{52}) \text{ erg s}^{-1}$ . The results are consistent with the magnetar engine hypothesis, namely, the spin energy of the newborn accreting magnetar can sustain the propeller mechanism and EM dipole spin-down emission energy in our LGRB sample.

## 5. CONCLUSIONS AND DISCUSSIONS

In Swift's 21 years of operation, the early-time afterglow emissions of GRBs have been revealed, and a rich trove of X-ray observation data have been collected, which provides valuable information for understanding the GRB central engine. A good fraction of the X-ray afterglows in GRBs pose a long-lasting plateau emission feature, which is thought to potentially energy injection into GRB's afterglow, and commonly taken as evidence of a newborn magnetar as the GRB central engine (Dai & Lu 1998a,b; Zhang & Mészáros 2001; Troja et al. 2007; Rowlinson et al. 2010, 2013, 2014; Fan et al. 2013a,b; Gompertz et al. 2013, 2014; Lü & Zhang 2014; Metzger & Piro 2014; Lü et al. 2015, 2018, 2019; Gao et al. 2016, 2017a,b; Lasky & Glampedakis 2016; Lasky et al. 2017; Ai et al. 2018, 2020; Lin & Lu 2019; Zou et al. 2019, 2021b; Lan et al. 2020a, 2021, 2025; Lin et al. 2020a; Sarin et al. 2020; Zhao et al. 2020; Ai & Zhang 2021; Xie et al. 2022a,b). In this work, by considering the  $R/I$  evolutionary effects during the magnetar spin-down process, we performed a systematic study in the propeller mechanism properties of newborn accreting magnetar by

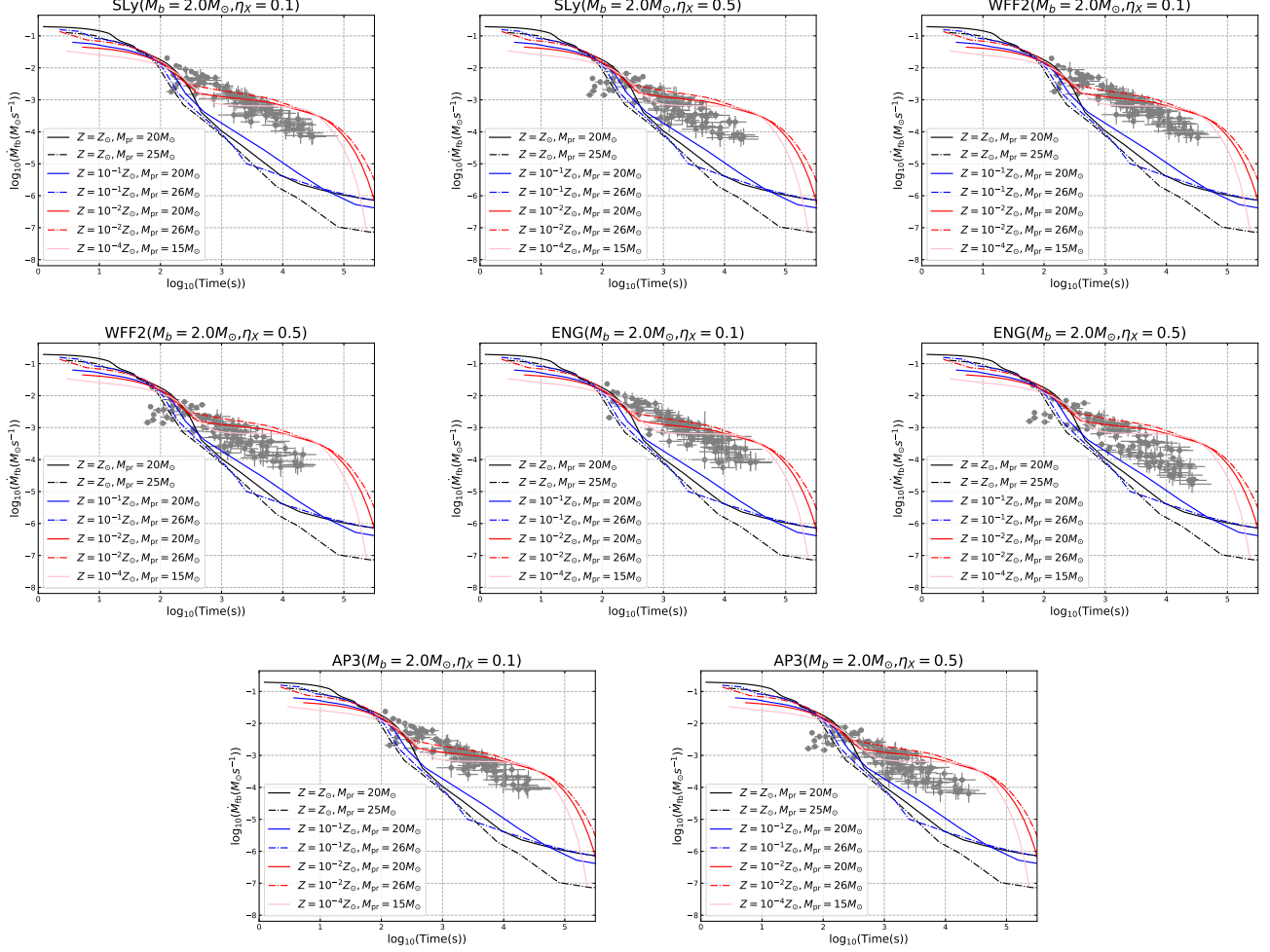


**Figure 5.** The evolution of the fallback rate of progenitor materials with different masses and metallicities onto the accretion disk for different EoSs and  $\eta_X$ . Lines of different colors and shapes represent different progenitor star masses and metallicities. The gray circles represent the fallback rate in our LGRB sample.

re-estimating the physical parameters of magnetar and investigating possible relations between the  $B_p$  and  $P_0$  based on the LGRB sample with X-ray plateau emission, and tried to constrain the accretion rate of accreting magnetar in different EoSs and X-ray radiative efficiencies, which is crucial to help us to understand the nature and physical environment of newborn accreting magnetar and its progenitor. In order to precisely diagnose the propeller properties of the newborn accreting magnetar, we invoked four samples of EoSs with bayonic masses  $M_b = 2.0 M_\odot$ , and two X-ray radiation efficiencies  $\eta_X = 0.1, 0.5$  to simultaneously constrain the accretion rate of accreting magnetar. Our main results can be summarized as follows:

- We found a universal correlation between the surface magnetic field  $B_p$  and the initial spin period  $P_0$  of newborn magnetar candidates based on 105 LGRBs with X-ray plateau emission sample in Lan et al. (2025). The overall  $B_p - P_0$  correlation can be approximately described as  $B_p \propto P_0^{1.30 \pm 0.16}$  for various (EoS,  $\eta_X$ ) combination scenarios, which seems to hint that the  $P_0$  estimated from plateau data could deviate from that of the magnetar at birth, but strongly links to the equilibrium spin period when the accreting magnetar has reached equilibrium in the magnetic propeller mechanism, which follow a positive correlation in agreement with  $B_p \propto P_{eq}^{7/6}$ .
- We found that the accretion rate of the accreting magnetar in our LGRB sample is in the range of  $\dot{M} \sim 10^{-5} - 10^{-2} M_\odot \text{ s}^{-1}$  by systematically incorporating  $R/I$  evolutionary effects and using the  $M_b - M_g$  transition relation in different EoSs and  $\eta_X$ . The accretion rate is one order of magnitude lower compared to the statistical results in Stratta et al. (2018) and Lin et al. (2020b), which used the constant  $R$ ,  $I$  and  $M_g$  for their LGRB sample. We

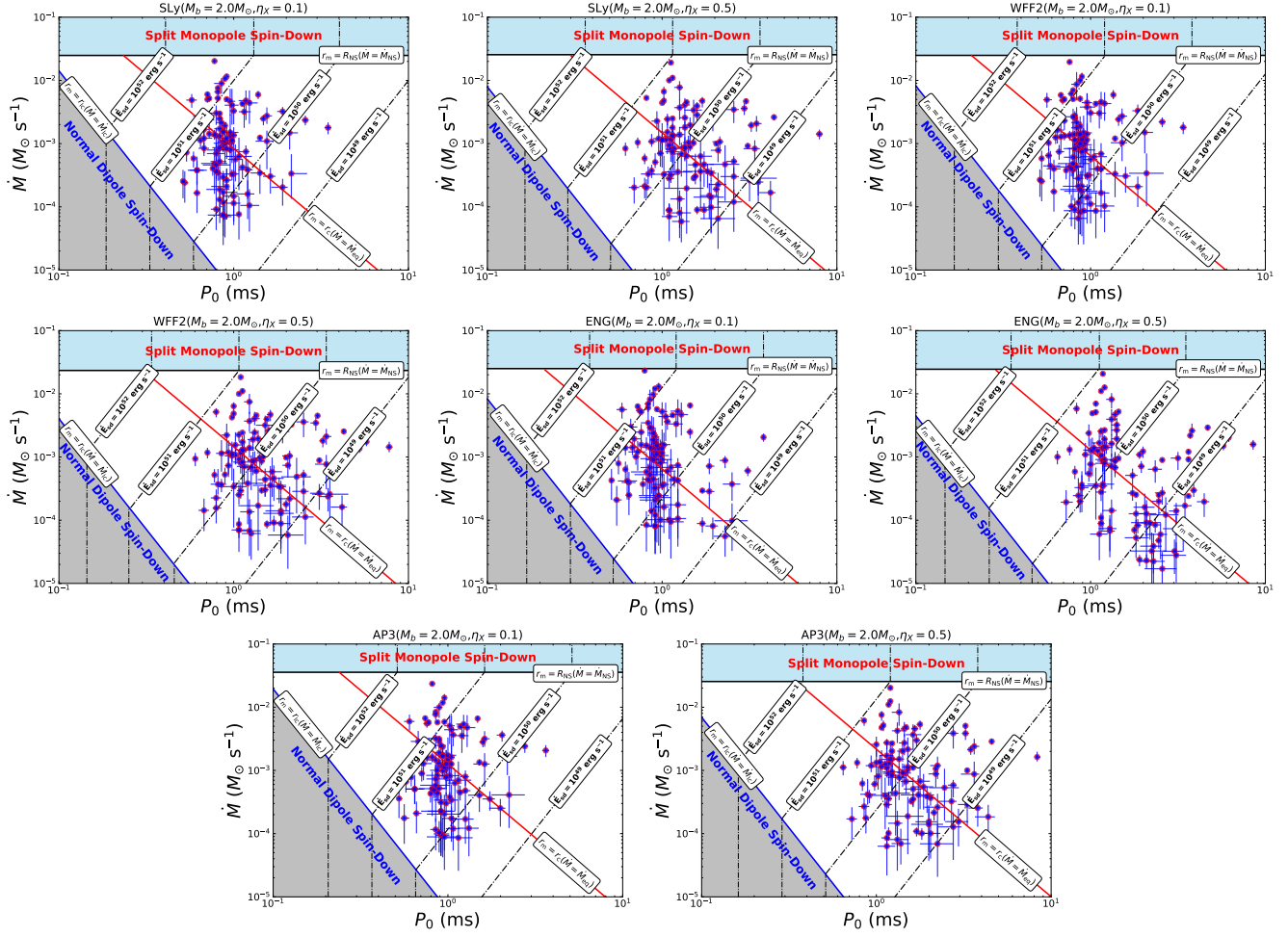


**Figure 6.** The spin-down evolution regimes of newborn magnetar for the parameter space of mass accretion rate  $\dot{M}$  and spin period  $P_0$  in different EoSs and  $\eta_X$ . The solid lines show accretion rates  $\dot{M} = \dot{M}_{\text{NS}}$  (black),  $\dot{M} = \dot{M}_{\text{eq}}$  (red), and  $\dot{M} = \dot{M}_{\text{ic}}$  (blue). The dashed-dotted lines show contours of constant spin-down luminosity  $\dot{E}_{\text{sd}}$ . The red solid circles are our LGRB sample. The skyblue shaded region and the gray shaded region represent the parameter space of split monopole spin-down evolution and the parameter space of normal dipole spin-down evolution, respectively.

suggest that the propeller properties of accreting magnetar are obtained by using the constant  $R/I$  scenario will yield a higher mass accretion rate, which may impair our understanding of the physical nature and its surroundings of accreting magnetar, and will further diminish the reliability of inverse inference about the physical properties of its progenitor.

- We found that the overall  $p$ -value of the K-S test for the derived accretion rates between different NS EoSs and different  $\eta_X$  can be approximately expressed as  $p_{\text{KS}} < 7.3 \times 10^{-1}$ ,  $p_{\text{KS}} < 5.3 \times 10^{-2}$ , respectively. The K-S test results indicate that there are no significant differences in the constrained mass accretion rates for different EoSs, and the constraints on magnitude of mass accretion rate seem to be independent of the EoS stiffness. However, there are systematic differences in the constrained mass accretion rates for different  $\eta_X$ , and with higher X-ray radiative efficiency, the constrained mass accretion rates tend to become larger.
- We found that no matter whether the radiative efficiency  $\eta_X$  is 0.1 or 0.5, most of the accreting magnetars in our GRB sample can actually survive the equilibrium spin period for two soft SLy and WFF2 EoSs ( $M_{\text{TOV}} = 2.05M_\odot, 2.20M_\odot$ ), and all the accreting magnetars in our GRB sample can actually survive the equilibrium spin period for two stiff EoSs ( $M_{\text{TOV}} = 2.24M_\odot, 2.39M_\odot$ ). The accretion masses of most newborn accreting magnetars in our LGRB sample are less than  $0.5M_\odot$  for various (EoS,  $\eta_X$ ) combination scenarios, which indicate that the majority of the nascent accreting magnetars in our GRB sample are able to survive until they reach the equilibrium

spin period, and will not collapse into black holes because their total mass after accreting materials to the magnetar surface does not exceed its maximum gravitational mass.

- We found that the fallback rate of progenitor envelope materials onto the magnetar accretion disk for our LGRB sample in various (EoS,  $\eta_X$ ) combination scenarios is compatible with the theoretical mass fallback rate of some low-metallicity massive progenitor stars such as those ones with ( $Z \lesssim 10^{-2} Z_\odot$ ,  $M \gtrsim 26 M_\odot$ ), ( $Z \lesssim 10^{-2} Z_\odot$ ,  $M \gtrsim 20 M_\odot$ ), ( $Z \lesssim 10^{-4} Z_\odot$ ,  $M \gtrsim 15 M_\odot$ ) based on the given the spin profile in Kumar et al. (2008) and density profile in Liu et al. (2018). These results suggest that the low-metallicity progenitors can provide enough material to satisfy the accretion requirements of the newborn accreting magnetar in our LGRB sample for various (EoS,  $\eta_X$ ) combinations. Furthermore, we found that all GRBs in our sample fall well within the region where the EM dipole radiation and the propeller mechanism jointly modulate the spin evolution of newborn magnetar, and the overall requirement for energy release  $\dot{E}_{\text{sd}} \subseteq (10^{49}, 10^{52}) \text{ erg s}^{-1}$ , which are consistent with the magnetar engine hypothesis for our LGRB sample.

In the end, we would like to point out that several uncertainties exist in the results we have obtained. Our results are based on a sample of LGRBs with X-ray plateau emission. This sample could suffer observational biases from the XRT fluctuation thresholds, and the magnetic dipole emission may be covered by bright jet afterglow emission, leading us to collect an incomplete sample. In other words, the data currently available for LGRBs with plateau emission are still limited, which may affect our results due to sample incompleteness. In addition, the above results are based on a simple method, with which we estimate the constant mass accretion rates from the  $B_p - P_0$  distribution inferred from the magnetar-powered models in given NS EoSs and X-ray radiative efficiency. However, in reality, we know very little about the NS EoS and X-ray radiative efficiency because of the unknown physical properties of matter under extreme conditions and radiation mechanisms of neutron stars, and in addition to the early-time accretion rate with constant rate, the late-time decay of accretion rate can also influence the spin period of the magnetar, and hence magnetar outflow can deviate from the magnetic dipole radiation luminosity evolution (Piro & Ott 2011; Metzger et al. 2018). These uncertainties in neutron star physics may introduce biases in our results. Furthermore, the physical conditions for a nascent NS in early stage would be very complicated, and some conditions may significantly alter the dipole radiation light curve, so that the  $R/I$  evolution effect we discussed here would be reduced or even completely suppressed, which may impair our estimates of the physical parameters of GRB magnetar and even demolish the  $B_p - P_0$  connections between the physical parameters of GRB magnetar. For instance, it has been proposed that the evolution of the inclination angle between the rotation and magnetic axes of the NS could markedly revise the X-ray emission (Çikintoğlu et al. 2020). Moreover, the nascent NS is likely to undergo free precession in the early stages of its lifetime when the rotation and magnetic axes of the system are not orthogonal to each other, which can lead to systematic fluctuations in the X-ray light curve (Suvorov & Kokkotas 2020, 2021; Zou et al. 2021a; Zou & Liang 2022; Zou & Cheng 2024; Zhang et al. 2024). The impact of these conditions on the constraints for the magnetar physical parameters warrants further investigation in the future to validate the authenticity of the  $B_p - P_0$  correlation.

Meanwhile, there are a couple of extra simplifying assumptions may also introduce uncertainty into our results. One key simplifying assumption in our analysis is the adoption of  $M_b = 2.0 M_\odot$  for all newborn magnetar in our LGRBs sample. This is because the primary research purpose of our work is to determine the true mass accretion rate of newborn accreting magnetar after incorporating  $R/I$  evolution effects and different gravitational masses. However, the  $R/I$  evolution effects depend on the rotational speed of the newborn magnetar. Only when the rotational speed of the newborn magnetar is approaching the break-up limit, its  $R/I$  values undergo an obvious evolution as the magnetar spins down, and it was found that only when the baryonic mass is  $2.0 M_\odot$  or greater can the  $R/I$  of newborn magnetar maintain a obvious evolution effect over the typical period  $P_0 \sim 1 \text{ ms}$  of the GRB magnetar central engine (Lan et al. 2021). Moreover, Lan et al. (2025) found that adopting a lower baryonic mass yields a smaller  $P_0$ , particularly when using a baryonic mass below  $2.0 M_\odot$ , which would lead to some  $P_0$  values in their LGRBs sample break the Keplerian break-up limit, and using a larger baryonic mass ( $M_b = 2.5 M_\odot$ ) would lead to some newborn magnetars rapidly collapse into black hole in the sample. Taking all these factors into account, we selected only a baryonic mass of  $2.0 M_\odot$  to determine the true mass accretion rate of newborn accreting magnetar after incorporating  $R/I$  evolution effects and different gravitational masses. We also re-examined the effect on the paper's final conclusions with a lower mass of  $1.4 M_\odot$ , as well as with a distribution of masses. Notably, the evolution effects of  $R/I$  can be neglected when using a lower mass. Based on  $\dot{M} \propto M_g^{-5/3}$  in Equation (8), a lower mass will lead to higher mass accretion rate. When using the constant  $R/I/M_g$  ( $M_g = 1.4 M_\odot$ ,  $R = 12 \text{ km}$ ,  $I = 0.35 M_g R^2$ ), we can obtain the range of mass accretion

rates  $10^{-4} M_{\odot} \text{ s}^{-1} < \dot{M} < 10^{-1} M_{\odot} \text{ s}^{-1}$  for our LGRBs sample, which are consistent with the statistical results in Stratta et al. (2018) and Lin et al. (2020b). This result aligns with the final conclusion of our paper, namely that adopting a constant  $R/I/M_g$  scenario for modeling the propeller regime in accreting magnetar results in a higher mass accretion rate.

Another key simplifying assumption in our analysis, as noted in Section 2, is the adoption of  $z = 1$  for the 62 LGRBs in our sample lacking redshift measurements. While this is a common practice in population studies of LGRBs (Berger et al. 2003; Xie et al. 2022a), it is crucial to assess the potential uncertainty this assumption introduces to our primary results. To quantitatively evaluate this, we repeated our entire analysis using only the sub-sample of 43 LGRBs with measured redshifts. We found a universal correlation still exists between the surface magnetic field  $B_p$  and the initial spin period  $P_0$ , even when using only the sub-sample of 43 LGRBs with measured redshifts. The slope of the overall  $B_p - P_0$  correlation changes from  $B_p \propto P_0^{1.30 \pm 0.16}$  (full sample) to  $B_p \propto P_0^{1.27 \pm 0.15}$  ( $z$ -known sample), which is still approximately consistent with the magnetic propeller model  $B_p \propto P_{\text{eq}}^{7/6}$ . The accretion rate of the accreting magnetar in the  $z$ -known sub-sample is also in the range of  $\dot{M} \sim 10^{-5} - 10^{-2} M_{\odot} \text{ s}^{-1}$  by systematically incorporating  $R/I$  evolutionary effects and using the  $M_b - M_g$  transition relation in different EoSs and  $\eta_X$ . For different NS EoSs and radiative efficiencies, the log-normal distributions in the  $z$ -known sub-sample can be described as  $\log \dot{M}^{(\text{SLy}, \eta_X=0.1)} / M_{\odot} \text{ s}^{-1} = -3.01 \pm 0.62$ ,  $\log \dot{M}^{(\text{SLy}, \eta_X=0.5)} / M_{\odot} \text{ s}^{-1} = -3.07 \pm 0.63$ ,  $\log \dot{M}^{(\text{WFF2}, \eta_X=0.1)} / M_{\odot} \text{ s}^{-1} = -3.01 \pm 0.62$ ,  $\log \dot{M}^{(\text{WFF2}, \eta_X=0.5)} / M_{\odot} \text{ s}^{-1} = -3.08 \pm 0.64$ ,  $\log \dot{M}^{(\text{ENG}, \eta_X=0.1)} / M_{\odot} \text{ s}^{-1} = -2.99 \pm 0.63$ ,  $\log \dot{M}^{(\text{ENG}, \eta_X=0.5)} / M_{\odot} \text{ s}^{-1} = -3.11 \pm 0.71$ ,  $\log \dot{M}^{(\text{AP3}, \eta_X=0.1)} / M_{\odot} \text{ s}^{-1} = -2.96 \pm 0.62$ ,  $\log \dot{M}^{(\text{AP3}, \eta_X=0.5)} / M_{\odot} \text{ s}^{-1} = -3.03 \pm 0.64$ . Most of the accreting magnetars in 43  $z$ -known samples can actually survive the equilibrium spin period for two soft SLy and WFF2 EoSs, and all the accreting magnetars in the  $z$ -known sub-sample can actually survive the equilibrium spin period for two stiff EoSs. The fallback rate of progenitor envelope materials onto the magnetar accretion disk for  $z$ -known sub-sample in various (EoS,  $\eta_X$ ) combination scenarios is also compatible with the theoretical mass fallback rate of some low-metallicity massive progenitor stars. The consistency between the two samples validates our approach of utilizing the larger dataset to maximize statistical precision without compromising accuracy.

From the theoretical point of view, such a universal  $B_p - P_0$  correlation for our LGRB sample in various (EoS,  $\eta_X$ ) combination scenarios is consistent with the  $B \propto P_{\text{eq}}^{7/6}$  relation for the magnetic propeller model. In an accreting magnetar propeller scenario, the materials at the edge of the accreting disk would flow into the magnetar polar caps along with the magnetic field lines and then form two accreting columns on the polar caps of newborn millisecond magnetar (known as “mountain”), which could lead to NS being deformed with an asymmetry in the mass distribution (Frank et al. 1992). In this scenario, the newborn accreting magnetar has a rapid time-varying quadrupole moment, allowing it to become the potential source of continuous GW radiation (Haskell et al. 2015; Haskell & Patruno 2017; Zhong et al. 2019; Sur & Haskell 2021; Huang et al. 2022). Moreover, accreting NSs should spin up as they gain angular momentum through mass accretion. However, observations reveal a significant lack of submillisecond pulsars in X-ray binaries, which observation phenomenon suggests that accreting NSs may achieve angular momentum balance through GW radiation, thus suppressing infinite acceleration of their spin (Bhattacharyya & Chakrabarty 2017). But, for an NS in X-ray binaries, the accretion rate is much lower, around the order of  $10^{-13} M_{\odot} \text{ yr}^{-1}$  (Papitto & Torres 2015; Jaodand et al. 2016), and their accretion mountain-induced deformation generates too weak GW radiation to be detected by the advanced LIGO/Virgo detector and the next generation ET detector (Konar et al. 2016). In contrast, the accretion columns of millisecond magnetar form under some extreme conditions, such as extremely high accretion rates, as expected for the newborn magnetar in GRBs with the order of  $10^{-5} M_{\odot} - 10^{-2} M_{\odot} \text{ s}^{-1}$  in our sample, and this resultant deformation could also lead to strong GW radiation (Zhong et al. 2019). Unfortunately, until now, we have not detected a single case of GW radiation in the remnants of LGRB with X-ray plateau emission. Furthermore, because of the interaction between the magnetar and its surrounding accretion disk during the propeller phase, the  $P_0$  that we have constrained using the X-ray plateau data may not be the true initial spin period but rather the equilibrium spin period via fallback accretion in the propeller model. In the future, we expect that the GW radiation associated with the X-ray plateau emission can be detected by Advanced LIGO and ET, which could not only offer the first smoking gun that a protomagnetar can serve as the central engine of GRBs, but could also play a crucial role in precisely constraining the true  $P_0$  and helping us to understand the nature and physical environment of newborn accreting magnetar and its progenitor.

**Table 1.** The center values and the best-fitting correlations between  $B_p$  and  $P_0$  for various scenarios.

EoS	$\log B_p$ (G)	$\log P_0$ (s)	$\log B_p - P_0$
$M_b = 2.0M_\odot, \eta_X = 0.1$			
SLy	$(14.24 \pm 0.37)$	$(-3.03 \pm 0.14)$	$\log B_p = (18.43 \pm 0.66) + (1.40 \pm 0.20) \log P_0$
WFF2	$(14.26 \pm 0.40)$	$(-3.04 \pm 0.14)$	$\log B_p = (18.37 \pm 0.64) + (1.37 \pm 0.21) \log P_0$
ENG	$(14.26 \pm 0.37)$	$(-3.01 \pm 0.15)$	$\log B_p = (18.20 \pm 0.61) + (1.34 \pm 0.20) \log P_0$
AP3	$(14.22 \pm 0.38)$	$(-3.01 \pm 0.14)$	$\log B_p = (18.39 \pm 0.65) + (1.41 \pm 0.21) \log P_0$
$M_b = 2.0M_\odot, \eta_X = 0.5$			
SLy	$(14.58 \pm 0.42)$	$(-2.82 \pm 0.21)$	$\log B_p = (17.92 \pm 0.37) + (1.21 \pm 0.13) \log P_0$
WFF2	$(14.61 \pm 0.42)$	$(-2.83 \pm 0.21)$	$\log B_p = (17.87 \pm 0.39) + (1.18 \pm 0.11) \log P_0$
ENG	$(14.54 \pm 0.41)$	$(-2.78 \pm 0.22)$	$\log B_p = (17.74 \pm 0.42) + (1.19 \pm 0.15) \log P_0$
AP3	$(14.56 \pm 0.42)$	$(-2.79 \pm 0.21)$	$\log B_p = (18.02 \pm 0.39) + (1.28 \pm 0.14) \log P_0$

**Table 2.** The characteristic parameters of newborn accreting magnetar in our sample for various EoSs and  $\eta_X$ .

EoS	$M_{\text{TOV}}$	$P_k$	$\alpha$	$\beta$	$(M_b, \eta_X)$	$P_0/P_k$	$A$	$M_g$	$R$	$\dot{M}$	$t_{\text{ev}}$
	$(M_\odot)$	(ms)	$(10^{-10} \text{ s}^{-\beta})$		$(M_\odot, -)$			$(M_\odot)$	(km)	$(M_\odot \text{ s}^{-1})$	(s)
SLy	2.05	0.55	2.31	-2.73	(2.0, 0.1)	$P_0 = 1.7P_k$	0.0730	1.77	14.185	$7.0 \times 10^{-5} - 2.0 \times 10^{-2}$	26–6149
					(2.0, 0.5)	$P_0 = 2.8P_k$	0.0756	1.76	11.912	$4.4 \times 10^{-5} - 1.4 \times 10^{-2}$	13–4127
WFF2	2.20	0.50	2.17	-2.69	(2.0, 0.1)	$P_0 = 1.8P_k$	0.0790	1.76	12.948	$4.2 \times 10^{-5} - 1.2 \times 10^{-2}$	27–6577
					(2.0, 0.5)	$P_0 = 3.0P_k$	0.0830	1.75	11.495	$3.7 \times 10^{-5} - 1.4 \times 10^{-2}$	12–4278
ENG	2.24	0.53	3.95	-2.68	(2.0, 0.1)	$P_0 = 1.8P_k$	0.0780	1.76	12.966	$2.9 \times 10^{-5} - 1.2 \times 10^{-2}$	24–6459
					(2.0, 0.5)	$P_0 = 3.1P_k$	0.0821	1.75	11.701	$1.7 \times 10^{-5} - 1.5 \times 10^{-2}$	12–5668
AP3	2.39	0.54	1.88	-2.78	(2.0, 0.1)	$P_0 = 1.8P_k$	0.0740	1.77	14.957	$7.9 \times 10^{-5} - 2.2 \times 10^{-2}$	23–5075
					(2.0, 0.5)	$P_0 = 3.0P_k$	0.0780	1.76	12.586	$4.2 \times 10^{-5} - 1.5 \times 10^{-2}$	11–4812

## ACKNOWLEDGMENTS

We thank the anonymous referee for a very thorough analysis of the original version and extremely helpful comments that have helped us to improve significantly the presentation of the paper. This work used data supplied by the UK *Swift* Science Data Centre at the University of Leicester. L.L. is supported by the China Postdoctoral Science Foundation (grant No. GZB20230765). L.Z. is supported by the Hebei Natural Science Foundation (grant No. A2024403004). J.L. is supported by the China Postdoctoral Science Foundation (grant No. GZC20240905). S.A. has received support from the Villum Foundation (Project No. 13164, PI: I. Tamborra). This work is supported by the National Natural Science Foundation of China (Projects 12373040, 12021003, 12303050, 12494573, 12563009, 12403047), the National SKA Program of China (2022SKA0130100) from the Fundamental Research Funds for the Central Universities, the Strategic Priority Research Program of the Chinese Academy of Sciences, Grant No. XDB0550401.

## REFERENCES

- Ai, S., Gao, H., Dai, Z.-G., et al. 2018, *ApJ*, 860, 57, doi: [10.3847/1538-4357/aac2b7](https://doi.org/10.3847/1538-4357/aac2b7)
- Ai, S., Gao, H., & Zhang, B. 2020, *ApJ*, 893, 146, doi: [10.3847/1538-4357/ab80bd](https://doi.org/10.3847/1538-4357/ab80bd)
- Ai, S., & Zhang, B. 2021, *ApJL*, 915, L11, doi: [10.3847/2041-8213/ac097d](https://doi.org/10.3847/2041-8213/ac097d)
- Akmal, A., & Pandharipande, V. R. 1997, *PhRvC*, 56, 2261, doi: [10.1103/PhysRevC.56.2261](https://doi.org/10.1103/PhysRevC.56.2261)
- Beloborodov, A. M. 1998, *MNRAS*, 297, 739, doi: [10.1046/j.1365-8711.1998.01530.x](https://doi.org/10.1046/j.1365-8711.1998.01530.x)
- Berger, E., Kulkarni, S. R., & Frail, D. A. 2003, *ApJ*, 590, 379, doi: [10.1086/374892](https://doi.org/10.1086/374892)

- Bernardini, M. G., Campana, S., Ghisellini, G., et al. 2013, *ApJ*, 775, 67, doi: [10.1088/0004-637X/775/1/67](https://doi.org/10.1088/0004-637X/775/1/67)
- Bhattacharyya, S., & Chakrabarty, D. 2017, *ApJ*, 835, 4, doi: [10.3847/1538-4357/835/1/4](https://doi.org/10.3847/1538-4357/835/1/4)
- Blandford, R. D., & Znajek, R. L. 1977, *MNRAS*, 179, 433, doi: [10.1093/mnras/179.3.433](https://doi.org/10.1093/mnras/179.3.433)
- Bucciantini, N., Metzger, B. D., Thompson, T. A., & Quataert, E. 2012, *MNRAS*, 419, 1537, doi: [10.1111/j.1365-2966.2011.19810.x](https://doi.org/10.1111/j.1365-2966.2011.19810.x)
- Bucciantini, N., Thompson, T. A., Arons, J., Quataert, E., & Del Zanna, L. 2006, *MNRAS*, 368, 1717, doi: [10.1111/j.1365-2966.2006.10217.x](https://doi.org/10.1111/j.1365-2966.2006.10217.x)
- Campana, S., Mangano, V., Blustin, A. J., et al. 2006, *Nature*, 442, 1008, doi: [10.1038/nature04892](https://doi.org/10.1038/nature04892)
- Çikintoğlu, S., Şaşmaz Muş, S., & Ekşi, K. Y. 2020, *MNRAS*, 496, 2183, doi: [10.1093/mnras/staa1556](https://doi.org/10.1093/mnras/staa1556)
- Chen, W.-X., & Beloborodov, A. M. 2007, *ApJ*, 657, 383, doi: [10.1086/508923](https://doi.org/10.1086/508923)
- Contopoulos, I., Kazanas, D., & Fendt, C. 1999, *ApJ*, 511, 351, doi: [10.1086/306652](https://doi.org/10.1086/306652)
- Corsi, A., & Mészáros, P. 2009, *ApJ*, 702, 1171, doi: [10.1088/0004-637X/702/2/1171](https://doi.org/10.1088/0004-637X/702/2/1171)
- Dai, Z. G., & Liu, R.-Y. 2012, *ApJ*, 759, 58, doi: [10.1088/0004-637X/759/1/58](https://doi.org/10.1088/0004-637X/759/1/58)
- Dai, Z. G., & Lu, T. 1998a, *A&A*, 333, L87, doi: [10.48550/arXiv.astro-ph/9810402](https://doi.org/10.48550/arXiv.astro-ph/9810402)
- . 1998b, *PhRvL*, 81, 4301, doi: [10.1103/PhysRevLett.81.4301](https://doi.org/10.1103/PhysRevLett.81.4301)
- Dall’Osso, S., Giacomazzo, B., Perna, R., & Stella, L. 2015, *ApJ*, 798, 25, doi: [10.1088/0004-637X/798/1/25](https://doi.org/10.1088/0004-637X/798/1/25)
- Dexter, J., & Kasen, D. 2013, *ApJ*, 772, 30, doi: [10.1088/0004-637X/772/1/30](https://doi.org/10.1088/0004-637X/772/1/30)
- Douchin, F., & Haensel, P. 2001, *A&A*, 380, 151, doi: [10.1051/0004-6361:20011402](https://doi.org/10.1051/0004-6361:20011402)
- Eichler, D., Livio, M., Piran, T., & Schramm, D. N. 1989, *Nature*, 340, 126, doi: [10.1038/340126a0](https://doi.org/10.1038/340126a0)
- Engvik, L., Osnes, E., Hjorth-Jensen, M., Bao, G., & Ostgaard, E. 1996, *ApJ*, 469, 794, doi: [10.1086/177827](https://doi.org/10.1086/177827)
- Fan, Y.-Z., Wu, X.-F., & Wei, D.-M. 2013a, *PhRvD*, 88, 067304, doi: [10.1103/PhysRevD.88.067304](https://doi.org/10.1103/PhysRevD.88.067304)
- Fan, Y.-Z., Yu, Y.-W., Xu, D., et al. 2013b, *ApJL*, 779, L25, doi: [10.1088/2041-8205/779/2/L25](https://doi.org/10.1088/2041-8205/779/2/L25)
- Foreman-Mackey, D., Hogg, D. W., Lang, D., & Goodman, J. 2013, *PASP*, 125, 306, doi: [10.1086/670067](https://doi.org/10.1086/670067)
- Frank, J., King, A., & Raine, D. 1992, *Accretion power in astrophysics.*, Vol. 21
- Gao, H., Ai, S.-K., Cao, Z.-J., et al. 2020, *Frontiers of Physics*, 15, 24603, doi: [10.1007/s11467-019-0945-9](https://doi.org/10.1007/s11467-019-0945-9)
- Gao, H., Cao, Z., & Zhang, B. 2017a, *ApJ*, 844, 112, doi: [10.3847/1538-4357/aa7d00](https://doi.org/10.3847/1538-4357/aa7d00)
- Gao, H., Lei, W.-H., Zou, Y.-C., Wu, X.-F., & Zhang, B. 2013, *NewAR*, 57, 141, doi: [10.1016/j.newar.2013.10.001](https://doi.org/10.1016/j.newar.2013.10.001)
- Gao, H., & Zhang, B. 2015, *ApJ*, 801, 103, doi: [10.1088/0004-637X/801/2/103](https://doi.org/10.1088/0004-637X/801/2/103)
- Gao, H., Zhang, B., & Lü, H.-J. 2016, *PhRvD*, 93, 044065, doi: [10.1103/PhysRevD.93.044065](https://doi.org/10.1103/PhysRevD.93.044065)
- Gao, H., Zhang, B., Lü, H.-J., & Li, Y. 2017b, *ApJ*, 837, 50, doi: [10.3847/1538-4357/aa5be3](https://doi.org/10.3847/1538-4357/aa5be3)
- Gehrels, N., Chincarini, G., Giommi, P., et al. 2004, *ApJ*, 611, 1005, doi: [10.1086/422091](https://doi.org/10.1086/422091)
- Gibson, S. L., Wynn, G. A., Gompertz, B. P., & O’Brien, P. T. 2017, *MNRAS*, 470, 4925, doi: [10.1093/mnras/stx1531](https://doi.org/10.1093/mnras/stx1531)
- . 2018, *MNRAS*, 478, 4323, doi: [10.1093/mnras/sty1363](https://doi.org/10.1093/mnras/sty1363)
- Gompertz, B. P., O’Brien, P. T., & Wynn, G. A. 2014, *MNRAS*, 438, 240, doi: [10.1093/mnras/stt2165](https://doi.org/10.1093/mnras/stt2165)
- Gompertz, B. P., O’Brien, P. T., Wynn, G. A., & Rowlinson, A. 2013, *MNRAS*, 431, 1745, doi: [10.1093/mnras/stt293](https://doi.org/10.1093/mnras/stt293)
- Haskell, B., & Patruno, A. 2017, *PhRvL*, 119, 161103, doi: [10.1103/PhysRevLett.119.161103](https://doi.org/10.1103/PhysRevLett.119.161103)
- Haskell, B., Priymak, M., Patruno, A., et al. 2015, *MNRAS*, 450, 2393, doi: [10.1093/mnras/stv726](https://doi.org/10.1093/mnras/stv726)
- Huang, J.-X., Lü, H.-J., Rice, J., & Liang, E.-W. 2022, *PhRvD*, 105, 103019, doi: [10.1103/PhysRevD.105.103019](https://doi.org/10.1103/PhysRevD.105.103019)
- Illarionov, A. F., & Sunyaev, R. A. 1975, *A&A*, 39, 185
- Jaodand, A., Archibald, A. M., Hessels, J. W. T., et al. 2016, *ApJ*, 830, 122, doi: [10.3847/0004-637X/830/2/122](https://doi.org/10.3847/0004-637X/830/2/122)
- Kobayashi, S. 2000, *ApJ*, 545, 807, doi: [10.1086/317869](https://doi.org/10.1086/317869)
- Koesterke, L., & Hamann, W. R. 1995, *A&A*, 299, 503
- Konar, S., Mukherjee, D., Bhattacharya, D., & Sarkar, P. 2016, *PhRvD*, 94, 104036, doi: [10.1103/PhysRevD.94.104036](https://doi.org/10.1103/PhysRevD.94.104036)
- Kumar, P., Narayan, R., & Johnson, J. L. 2008, *MNRAS*, 388, 1729, doi: [10.1111/j.1365-2966.2008.13493.x](https://doi.org/10.1111/j.1365-2966.2008.13493.x)
- Kumar, P., & Zhang, B. 2015, *PhR*, 561, 1, doi: [10.1016/j.physrep.2014.09.008](https://doi.org/10.1016/j.physrep.2014.09.008)
- Lan, L., Gao, H., Ai, S., & Li, S.-Z. 2021, *ApJ*, 919, 14, doi: [10.3847/1538-4357/ac167d](https://doi.org/10.3847/1538-4357/ac167d)
- Lan, L., Gao, H., Ai, S., et al. 2025, *ApJS*, 280, 45, doi: [10.3847/1538-4365/ade4](https://doi.org/10.3847/1538-4365/ade4)
- Lan, L., Lü, H.-J., Rice, J., & Liang, E.-W. 2020a, *ApJ*, 890, 99, doi: [10.3847/1538-4357/ab6c64](https://doi.org/10.3847/1538-4357/ab6c64)
- Lan, L., Lu, R.-J., Lü, H.-J., et al. 2020b, *MNRAS*, 492, 3622, doi: [10.1093/mnras/staa044](https://doi.org/10.1093/mnras/staa044)
- Lan, L., Lü, H.-J., Zhong, S.-Q., et al. 2018, *ApJ*, 862, 155, doi: [10.3847/1538-4357/aacda6](https://doi.org/10.3847/1538-4357/aacda6)
- Lan, L., Gao, H., Li, A., et al. 2023, *ApJL*, 949, L4, doi: [10.3847/2041-8213/accf93](https://doi.org/10.3847/2041-8213/accf93)

- Lasky, P. D., & Glampedakis, K. 2016, MNRAS, 458, 1660, doi: [10.1093/mnras/stw435](https://doi.org/10.1093/mnras/stw435)
- Lasky, P. D., Haskell, B., Ravi, V., Howell, E. J., & Coward, D. M. 2014, PhRvD, 89, 047302, doi: [10.1103/PhysRevD.89.047302](https://doi.org/10.1103/PhysRevD.89.047302)
- Lasky, P. D., Leris, C., Rowlinson, A., & Glampedakis, K. 2017, ApJL, 843, L1, doi: [10.3847/2041-8213/aa79a7](https://doi.org/10.3847/2041-8213/aa79a7)
- Lee, H. K., Wijers, R. A. M. J., & Brown, G. E. 2000, PhR, 325, 83, doi: [10.1016/S0370-1573\(99\)00084-8](https://doi.org/10.1016/S0370-1573(99)00084-8)
- Lei, W. H., Wang, D. X., Zhang, L., et al. 2009, ApJ, 700, 1970, doi: [10.1088/0004-637X/700/2/1970](https://doi.org/10.1088/0004-637X/700/2/1970)
- Lei, W.-H., Zhang, B., & Liang, E.-W. 2013, ApJ, 765, 125, doi: [10.1088/0004-637X/765/2/125](https://doi.org/10.1088/0004-637X/765/2/125)
- Li, L.-X. 2000, ApJL, 533, L115, doi: [10.1086/312616](https://doi.org/10.1086/312616)
- Li, S.-Z., Yu, Y.-W., Gao, H., & Zhang, B. 2021, ApJ, 907, 87, doi: [10.3847/1538-4357/abcc70](https://doi.org/10.3847/1538-4357/abcc70)
- Lin, J., & Lu, R.-J. 2019, ApJ, 871, 160, doi: [10.3847/1538-4357/aaf72f](https://doi.org/10.3847/1538-4357/aaf72f)
- Lin, J., Lu, R.-J., Lin, D.-B., & Wang, X.-G. 2020a, ApJ, 895, 46, doi: [10.3847/1538-4357/ab88a7](https://doi.org/10.3847/1538-4357/ab88a7)
- Lin, W., Wang, X., Wang, L., & Dai, Z. 2021, ApJL, 914, L2, doi: [10.3847/2041-8213/ac004a](https://doi.org/10.3847/2041-8213/ac004a)
- Lin, W. L., Wang, X. F., Wang, L. J., & Dai, Z. G. 2020b, ApJL, 903, L24, doi: [10.3847/2041-8213/abc254](https://doi.org/10.3847/2041-8213/abc254)
- Liu, T., Gu, W.-M., & Zhang, B. 2017, NewAR, 79, 1, doi: [10.1016/j.newar.2017.07.001](https://doi.org/10.1016/j.newar.2017.07.001)
- Liu, T., Song, C.-Y., Zhang, B., Gu, W.-M., & Heger, A. 2018, ApJ, 852, 20, doi: [10.3847/1538-4357/aa9e4f](https://doi.org/10.3847/1538-4357/aa9e4f)
- Lü, H.-J., Lan, L., & Liang, E.-W. 2019, ApJ, 871, 54, doi: [10.3847/1538-4357/aaf71d](https://doi.org/10.3847/1538-4357/aaf71d)
- Lü, H.-J., & Zhang, B. 2014, ApJ, 785, 74, doi: [10.1088/0004-637X/785/1/74](https://doi.org/10.1088/0004-637X/785/1/74)
- Lü, H.-J., Zhang, B., Lei, W.-H., Li, Y., & Lasky, P. D. 2015, ApJ, 805, 89, doi: [10.1088/0004-637X/805/2/89](https://doi.org/10.1088/0004-637X/805/2/89)
- Lü, H.-J., Zou, L., Lan, L., & Liang, E.-W. 2018, MNRAS, 480, 4402, doi: [10.1093/mnras/sty2176](https://doi.org/10.1093/mnras/sty2176)
- Lyford, N. D., Baumgarte, T. W., & Shapiro, S. L. 2003, ApJ, 583, 410, doi: [10.1086/345350](https://doi.org/10.1086/345350)
- MacFadyen, A. I., & Woosley, S. E. 1999, ApJ, 524, 262, doi: [10.1086/307790](https://doi.org/10.1086/307790)
- Mészáros, P. 2002, ARA&A, 40, 137, doi: [10.1146/annurev.astro.40.060401.093821](https://doi.org/10.1146/annurev.astro.40.060401.093821)
- Mészáros, P., & Rees, M. J. 1997, ApJ, 476, 232, doi: [10.1086/303625](https://doi.org/10.1086/303625)
- Metzger, B. D., Beniamini, P., & Giannios, D. 2018, ApJ, 857, 95, doi: [10.3847/1538-4357/aab70c](https://doi.org/10.3847/1538-4357/aab70c)
- Metzger, B. D., Giannios, D., Thompson, T. A., Bucciantini, N., & Quataert, E. 2011, MNRAS, 413, 2031, doi: [10.1111/j.1365-2966.2011.18280.x](https://doi.org/10.1111/j.1365-2966.2011.18280.x)
- Metzger, B. D., Margalit, B., Kasen, D., & Quataert, E. 2015, MNRAS, 454, 3311, doi: [10.1093/mnras/stv2224](https://doi.org/10.1093/mnras/stv2224)
- Metzger, B. D., & Piro, A. L. 2014, MNRAS, 439, 3916, doi: [10.1093/mnras/stu247](https://doi.org/10.1093/mnras/stu247)
- Metzger, B. D., Quataert, E., & Thompson, T. A. 2008, MNRAS, 385, 1455, doi: [10.1111/j.1365-2966.2008.12923.x](https://doi.org/10.1111/j.1365-2966.2008.12923.x)
- Michel, F. C. 1988, Nature, 333, 644, doi: [10.1038/333644a0](https://doi.org/10.1038/333644a0)
- Mushtukov, A. A., Ingram, A., Middleton, M., Nagirner, D. I., & van der Klis, M. 2019, MNRAS, 484, 687, doi: [10.1093/mnras/sty3525](https://doi.org/10.1093/mnras/sty3525)
- Paczynski, B. 1986, ApJL, 308, L43, doi: [10.1086/184740](https://doi.org/10.1086/184740)
- Papitto, A., & Torres, D. F. 2015, ApJ, 807, 33, doi: [10.1088/0004-637X/807/1/33](https://doi.org/10.1088/0004-637X/807/1/33)
- Parfrey, K., Spitkovsky, A., & Beloborodov, A. M. 2016, ApJ, 822, 33, doi: [10.3847/0004-637X/822/1/33](https://doi.org/10.3847/0004-637X/822/1/33)
- Pe'er, A., Mészáros, P., & Rees, M. J. 2006, ApJ, 642, 995, doi: [10.1086/501424](https://doi.org/10.1086/501424)
- Piro, A. L., & Ott, C. D. 2011, ApJ, 736, 108, doi: [10.1088/0004-637X/736/2/108](https://doi.org/10.1088/0004-637X/736/2/108)
- Planck Collaboration, Aghanim, N., Akrami, Y., et al. 2020, A&A, 641, A6, doi: [10.1051/0004-6361/201833910](https://doi.org/10.1051/0004-6361/201833910)
- Popham, R., Woosley, S. E., & Fryer, C. 1999, ApJ, 518, 356, doi: [10.1086/307259](https://doi.org/10.1086/307259)
- Rees, M. J., & Meszaros, P. 1994, ApJL, 430, L93, doi: [10.1086/187446](https://doi.org/10.1086/187446)
- Rees, M. J., & Mészáros, P. 2005, ApJ, 628, 847, doi: [10.1086/430818](https://doi.org/10.1086/430818)
- Rowlinson, A., Gompertz, B. P., Dainotti, M., et al. 2014, MNRAS, 443, 1779, doi: [10.1093/mnras/stu1277](https://doi.org/10.1093/mnras/stu1277)
- Rowlinson, A., O'Brien, P. T., Metzger, B. D., Tanvir, N. R., & Levan, A. J. 2013, MNRAS, 430, 1061, doi: [10.1093/mnras/sts683](https://doi.org/10.1093/mnras/sts683)
- Rowlinson, A., O'Brien, P. T., Tanvir, N. R., et al. 2010, MNRAS, 409, 531, doi: [10.1111/j.1365-2966.2010.17354.x](https://doi.org/10.1111/j.1365-2966.2010.17354.x)
- Ruffert, M., Janka, H. T., Takahashi, K., & Schaefer, G. 1997, A&A, 319, 122, doi: [10.48550/arXiv.astro-ph/9606181](https://doi.org/10.48550/arXiv.astro-ph/9606181)
- Sari, R., Piran, T., & Narayan, R. 1998, ApJL, 497, L17, doi: [10.1086/311269](https://doi.org/10.1086/311269)
- Sarin, N., Lasky, P. D., & Ashton, G. 2020, MNRAS, 499, 5986, doi: [10.1093/mnras/staa3090](https://doi.org/10.1093/mnras/staa3090)
- Spitkovsky, A. 2006, ApJL, 648, L51, doi: [10.1086/507518](https://doi.org/10.1086/507518)
- Stergioulas, N., & Friedman, J. L. 1995, ApJ, 444, 306, doi: [10.1086/175605](https://doi.org/10.1086/175605)
- Stratta, G., Dainotti, M. G., Dall'Osso, S., Hernandez, X., & De Cesare, G. 2018, ApJ, 869, 155, doi: [10.3847/1538-4357/aadd8f](https://doi.org/10.3847/1538-4357/aadd8f)
- Sur, A., & Haskell, B. 2021, MNRAS, 502, 4680, doi: [10.1093/mnras/stab307](https://doi.org/10.1093/mnras/stab307)

- Suvorov, A. G., & Kokkotas, K. D. 2020, *ApJL*, 892, L34, doi: [10.3847/2041-8213/ab8296](https://doi.org/10.3847/2041-8213/ab8296)
- . 2021, *MNRAS*, 502, 2482, doi: [10.1093/mnras/stab153](https://doi.org/10.1093/mnras/stab153)
- Thompson, C. 1994, *MNRAS*, 270, 480, doi: [10.1093/mnras/270.3.480](https://doi.org/10.1093/mnras/270.3.480)
- Troja, E., Cusumano, G., O'Brien, P. T., et al. 2007, *ApJ*, 665, 599, doi: [10.1086/519450](https://doi.org/10.1086/519450)
- Usov, V. V. 1992, *Nature*, 357, 472, doi: [10.1038/357472a0](https://doi.org/10.1038/357472a0)
- Wiringa, R. B., Fiks, V., & Fabrocini, A. 1988, *PhRvC*, 38, 1010, doi: [10.1103/PhysRevC.38.1010](https://doi.org/10.1103/PhysRevC.38.1010)
- Woosley, S. E. 1993, *ApJ*, 405, 273, doi: [10.1086/172359](https://doi.org/10.1086/172359)
- Woosley, S. E., & Bloom, J. S. 2006, *ARA&A*, 44, 507, doi: [10.1146/annurev.astro.43.072103.150558](https://doi.org/10.1146/annurev.astro.43.072103.150558)
- Woosley, S. E., & Heger, A. 2006, *ApJ*, 637, 914, doi: [10.1086/498500](https://doi.org/10.1086/498500)
- Xiao, D., & Dai, Z.-G. 2019, *ApJ*, 878, 62, doi: [10.3847/1538-4357/ab12da](https://doi.org/10.3847/1538-4357/ab12da)
- Xie, L., Wei, D.-M., Wang, Y., & Jin, Z.-P. 2022a, *ApJ*, 934, 125, doi: [10.3847/1538-4357/ac7c13](https://doi.org/10.3847/1538-4357/ac7c13)
- Xie, L., Wei, D.-M., Wang, Y., Li, L., & Jin, Z.-P. 2022b, *MNRAS*, 513, 1365, doi: [10.1093/mnras/stac859](https://doi.org/10.1093/mnras/stac859)
- Xu, K., & Li, X.-D. 2019, *ApJ*, 877, 138, doi: [10.3847/1538-4357/ab1902](https://doi.org/10.3847/1538-4357/ab1902)
- Yang, Z., Lü, H.-J., Yang, X., Shen, J., & Yi, S.-X. 2024, *MNRAS*, 535, 2482, doi: [10.1093/mnras/stae2496](https://doi.org/10.1093/mnras/stae2496)
- Yu, W.-Y., Lü, H.-J., Yang, X., Lan, L., & Yang, Z. 2024, *ApJ*, 962, 6, doi: [10.3847/1538-4357/ad1756](https://doi.org/10.3847/1538-4357/ad1756)
- Zhang, B. 2011, *Comptes Rendus Physique*, 12, 206, doi: [10.1016/j.crhy.2011.03.004](https://doi.org/10.1016/j.crhy.2011.03.004)
- . 2018, *The Physics of Gamma-Ray Bursts*, doi: [10.1017/9781139226530](https://doi.org/10.1017/9781139226530)
- Zhang, B., & Mészáros, P. 2001, *ApJL*, 552, L35, doi: [10.1086/320255](https://doi.org/10.1086/320255)
- . 2004, *International Journal of Modern Physics A*, 19, 2385, doi: [10.1142/S0217751X0401746X](https://doi.org/10.1142/S0217751X0401746X)
- Zhang, B., & Yan, H. 2011, *ApJ*, 726, 90, doi: [10.1088/0004-637X/726/2/90](https://doi.org/10.1088/0004-637X/726/2/90)
- Zhang, B., Zhong, S.-Q., Li, L., & Dai, Z.-G. 2024, *ApJ*, 977, 206, doi: [10.3847/1538-4357/ad9005](https://doi.org/10.3847/1538-4357/ad9005)
- Zhao, L., Chen, M., Wu, F., et al. 2025, *ApJ*, 979, 186, doi: [10.3847/1538-4357/ada0b9](https://doi.org/10.3847/1538-4357/ada0b9)
- Zhao, L., Liu, L., Gao, H., et al. 2020, *ApJ*, 896, 42, doi: [10.3847/1538-4357/ab8f91](https://doi.org/10.3847/1538-4357/ab8f91)
- Zhong, S.-Q., Dai, Z.-G., & Li, X.-D. 2019, *PhRvD*, 100, 123014, doi: [10.1103/PhysRevD.100.123014](https://doi.org/10.1103/PhysRevD.100.123014)
- Zhong, S.-Q., Li, L., Xiao, D., et al. 2024, *ApJL*, 963, L26, doi: [10.3847/2041-8213/ad2852](https://doi.org/10.3847/2041-8213/ad2852)
- Zou, L., & Cheng, J.-G. 2024, *ApJ*, 973, 126, doi: [10.3847/1538-4357/ad6dd9](https://doi.org/10.3847/1538-4357/ad6dd9)
- Zou, L., & Liang, E.-W. 2022, *MNRAS*, 513, L89, doi: [10.1093/mnrasl/slac040](https://doi.org/10.1093/mnrasl/slac040)
- Zou, L., Zheng, T.-C., Yang, X., et al. 2021a, *ApJL*, 921, L1, doi: [10.3847/2041-8213/ac2ee4](https://doi.org/10.3847/2041-8213/ac2ee4)
- Zou, L., Zhou, Z.-M., Xie, L., et al. 2019, *ApJ*, 877, 153, doi: [10.3847/1538-4357/ab17dc](https://doi.org/10.3847/1538-4357/ab17dc)
- Zou, L., Liang, E.-W., Zhong, S.-Q., et al. 2021b, *MNRAS*, 508, 2505, doi: [10.1093/mnras/stab2766](https://doi.org/10.1093/mnras/stab2766)